Determining Steel Weld Qualification and Performance for Hydrogen Pipelines *

Phase I Report to

The US Department of Transportation, Pipeline and Hazardous Materials Safety Administration,

693JK319000013

By

M.J. Connolly, M.L. Martin, R.L. Amaro, Z.N. Buck, N. Moser, E. Lucon, D.S. Lauria, P.E. Bradley, and A.J. Slifka

February 28th, 2023

Abstract

This report details the results of Phase I of the DOT/PHMSA sponsored work on “Determining Steel Weld Qualification and Performance for Hydrogen Pipelines”. In this work, the goals of Phase I were 1) to perform a literature review of steel weld qualification and performance for hydrogen pipelines, 2) to form a committee of industry and subject matter experts, 3) to review the current codes and standards related to pipeline steel welds, 4) to review the regulatory requirements and limits for materials under 49 CFR Part 192, and 5) to identify materials necessary to inform advancement of 1-4.

A research plan was developed that takes a three-pronged approach to determining weld and HAZ performance for hydrogen pipelines: 1) survey industry for a wide spectrum of typical pipeline welds, 2) use Gleeble to simulate HAZ microstructures, and 3) systematically study standard and exploratory weld filler materials. During Phase II, NIST will perform Charpy impact tests, fracture toughness tests in air, in hydrogen gas, and in hydrogen/methane blends, hardness mapping, and microstructure characterization over a wide range of welds and HAZs.

Material procurement was begun through connections formed through the committee of subject matter experts and others within API 1104. At the submission of this Phase I report, NIST has procured ten pipes with welds formed using filler materials and six pipes with welds formed without filler materials. Additionally, NIST has formed collaborations with the Colorado School of Mines to perform Gleeble welding simulations as well as mechanized welding using a range of filler materials.

Keywords: ASME B31.12, 49 CFR Part 192, Hydrogen-assisted cracking, hydrogen embrittlement, fracture, Charpy, fatigue, fatigue crack growth rate, microstructure, pipeline steel.

Table of Contents

List of Figures

Acknowledgements

We wish to thank Rick Noecker, Paul Spielbauer, and Ben Pierce for fruitful conversations on the current state of pipelines and welds, including for hydrogen service. Additionally, we would like to thank Doug Stalheim, Nathan Regdos, and Dan Moers for support through material procurement for Phase II of this study.

Executive Summary

ASME B31.12 code provides direction for designing pipelines for high pressure gaseous service. Welding of these pipelines is explicitly covered in B31.12, however specific weld qualification is relegated to API 1104, which does not cover hydrogen explicitly. Furthermore, although regulations for hydrogen pipelines are implicitly covered by 49CFR Part 192 "Transportation of Natural and Other Gas by Pipeline: Minimum Federal Safety Standards" as an "other gas", hydrogen is not explicitly referenced. This is potentially a severe issue, as steel microstructures created during welding processes may be suitable for natural gas transport but lose significant ductility in the presence of hydrogen. We propose an extensive testing matrix to investigate the mechanical performance of microstructures generated at and near welds in pipelines for hydrogen and blended hydrogen/natural gas service. The data from this testing matrix will be used to update ASME B31.12 and provide guidance for explicit incorporation of hydrogen within 49CFR Part 192. Additionally, we have isolated some specific key issues within ASME B31.12, API 1104, and 49 CFR Part 192 for qualifying and assessing the performance of welds for hydrogen performance, as summarized below:

B31.12

- **Minimum Charpy requirements for the welds and HAZs are significantly less than the minimum Charpy requirements for the base metal, for all but small diameter pipes with very thick walls.**
- **A potential code change has been suggested within the BPVC to modify Article KD-1040 to allow for the use of either ASTM E1681 or ASTM E1820 when determining a materials crack threshold resistance in hydrogen environments.**
- **There is now a push to provide a third option, Option C, within ASME B31.12 to allow for increased operating pressure. Option C would provide a suggested range of microstructures that are shown to be least susceptible to degradation by hydrogen. Before an Option C could be incorporated in ASME B31.12, it is necessary to perform sufficient characterization for a large range of microstructures on the in-air ductility attributes (Charpy transition curves and the fracture toughness, the carbon equivalent, the maximum hardness, and the centerline segregation) and a correlation of that information to performance in hydrogen.**

API 1104

- **The prescribed specimen placement for Charpy impact testing necessarily has the crack path moving through multiple microstructures, including the weld metal, base metal, and all of the different HAZ zones (CG-HAZ, FG-HAZ, and IC-HAZ). In one example case (Example Case #1 in this report), the API 1104 assessment of material performance through Charpy testing was not sufficient for assessment of the effect of hydrogen, as the lowest toughness material would not be sufficiently isolated at the Charpy v-notch.**

<u>49 CFR Part 192</u>

- **Of note, the derating factor *T* above 400 F (204 C) ranges from 0.900 – 0.867. Because 49 CFR Part 192 does not explicitly address hydrogen, High Temperature Hydrogen Attack (HTHA), a mechanism of hydrogen-assisted damage which severely degrades steels at temperatures above 400 F, is not fully addressed with the derating factor *T*, as HTHA begins to severely degrade steels at temperatures above 400 F. Although HTHA is outside of the scope of this project, this highlights the potential issues that may arise by not explicitly addressing hydrogen in 49 CFR Part 192.**
- **ASME B31.12 is only referenced indirectly through 49 CFR Part 192, within 192.112 b-1-iii, and only pipelines using a maximum alternative operating pressure will be required to utilize the material design factor H_f, though ASME B31.12 utilizes H_f for all design pressures under ASME B31.12 Pl-3.7.1 Option A.**
- **While 49 CFR Part 192 limits the maximum hardness at the seam weld to 280 Vickers, ASME B31.12 limits the hardness to 235 Vickers.**

Introduction

Pipelines remain the safest and most efficient means for transporting natural gas and hydrogen. However, the welding process which forms material into pipes (seam welds), connects different sections of pipes along the transmission line (girth welds), or patches damaged pipeline sections (repair welds) can locally modify the chemistry and microstructure compared to the base pipeline material. Hydrogen is known to deteriorate mechanical performance of steels ("hydrogen embrittlement"), which can significantly reduce the expected lifetime of pipelines or lead to premature failure. To maintain safe operation of pipelines for hydrogen or hydrogen/natural gas blends, it is critical to assess weld qualification requirements considering new pipeline materials and weld processes and develop assessment parameters for evaluating the integrity of pipelines to be installed for transmission of hydrogen and natural gas blends.

The American Petroleum Institute (API) Standard 1104 [1], API Standard 5L[2], and the American Society of Mechanical Engineers (ASME) Standards B31.8 [3], and B31.12 [4] cover the design, materials, maintenance, and execution of integrity programs for pipelines. However, there are some gaps in knowledge and requirements in these standards when it comes to welds. For example, weld qualification is not yet completely covered by ASME B31.12. A thorough review of these standards is necessary to identify gaps of knowledge and requirements for welds in pipelines intended for hydrogen or hydrogen/natural gas blends.

The current, primary focus of industry is on hydrogen blends up to 20%, so the assessment of welds for blended service should first focus on this blend concentration, and subsequently address higher concentrations for future applications. Hydrogen/methane blends have primarily been used as a surrogate gas to study hydrogen/natural gas blends. Existing natural gas pipelines are regulated under U.S. Department of Transportation (DOT) regulations in Title 49, Part 192 of the Code of Federal Regulations (49 CFR Part 192) [5]. Therefore, any updates to API 1104, API 5L, ASME B31.8, or ASME B31.12 and weld qualification requirements must be compared with 49 CFR Part 192 to maintain pipeline safety. Currently, 49 CFR Part 192 briefly refers to B31.8, while B31.12 is not referred to explicitly by 49 CFR Part 192. The effectiveness and pertinence of B31.8 and B31.12 as it relates to 49 CFR Part 192 must be evaluated to determine if further incorporation of these standards would lead to better pipeline safety.

The construction of modern pipelines begins with line pipe [6]. Figure 1 depicts the taxonomy of modern line pipe [7]. Modern line pipe is delivered either as seamless or seamed. The majority of seamless pipe will be delivered in a quenched and tempered condition, however the line pipe may also come as-rolled or in a normalized condition. Normalization is the process of heating the line pipe above 1600 F and allowing to air cool, which creates a fine-grain, homogeneous microstructure while reducing residual stresses as well as the phase fraction of bainite, untampered martensite. Seamed pipe is most often manufactured using thermomechanically-controlled processing (TMCP) of a steel plate or strip which is bent to the prescribed diameter and welded using either longitudinal or helical welding seams. The typical welding process for both longitudinal and helical welding is submerged arc welding (SAWL or SAWH for longitudinal or helical, respectively). Longitudinal welding is also done using High-frequency welding (HFW), which is a weld-process without the use of filler material.

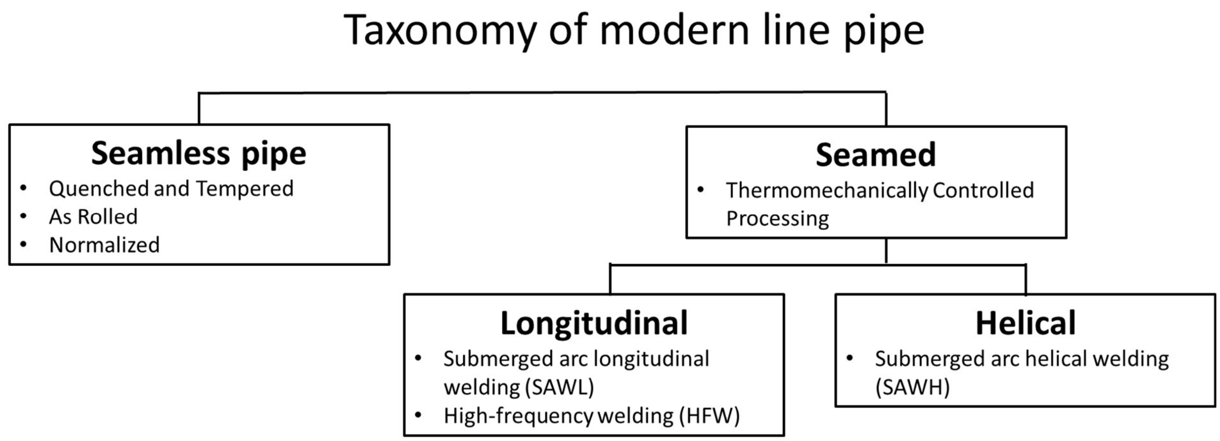

Figure 1: Taxonomy of modern line pipe.

Line pipe is delivered to the pipeline construction site typically in 40-foot sections, which are then butted together and welded on-site to connect each section to the main pipeline using girth welds. To reduce the number of welds performed on-site, often these 40-foot sections are connected prior to placement in the trench, using "double-joint" welds. Typical welding procedures for double-joint welds are submerged arc welding (SAW) and gas metal arc welding (GMAW). These 80-foot sections are then girth-welded to the main pipeline ("mainline" welds) using shielded metal arc welding (SMAW), gas tungsten arc welding (GTAW) or GMAW. Less frequently, these welds are formed using flux-cored arc welding (FCAW), and combinations of welding types are sometimes used for single welds. When a new pipeline is connected to an existing pipeline, a tee is created, and the new mainline weld is connected using "tie-in" welds. Tie-in welds are typically created using SMAW or FCAW procedures.

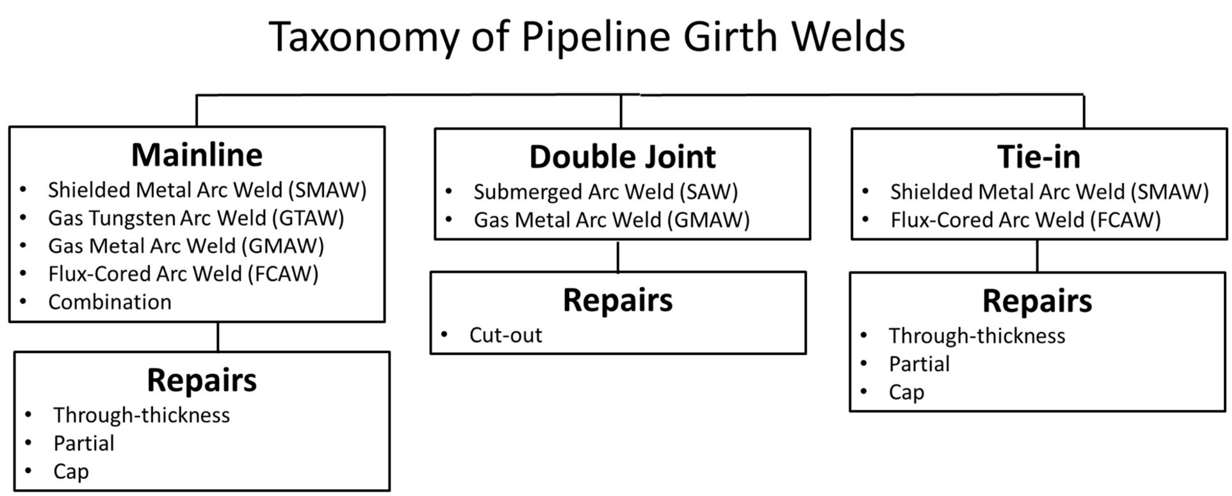

Figure 2: Taxonomy of modern pipeline girth welds.

Double-joint welds are typically created using a mechanized process. Once the mechanized welding procedure is established and proved, the failure rate of double-joint welds is near zero percent. However, if the parameters of the mechanized welding process are not optimized, the failure rate can be 100%. That is, mechanized welds create nearly identical welds each pass: if one is good, they are typically all good. Mainline welds, on the other hand, are performed by certified welders. The failure rate for these non-mechanized welds are typically between 3%-10%. When failures occur in double-joint welds, repairs are typically done by cutting out and re-doing the weld. On the other hand, repairs to mainline welds are performed with the pipeline in-place. Repairs to mainline pipe welds can be repairs to the entire weld ("through-thickness") or limited to only the root or cap ("partial" or "cap"). Figure 2 depicts this "taxonomy of pipeline girth welds".

Given the large number of options available for line pipe material, line pipe processing, and pipeline welding procedures, a large amount of data is required to adequately provide guidance for pipeline welding for hydrogen or hydrogen/natural gas blend service. The Materials Performance in Hydrogen Project within the National Institute of Standards and Technology (Applied Chemicals and Materials Division, Structural Materials Group) is uniquely poised to address gaps in knowledge related to welds in the existing pipeline codes and standards. NIST has an existing set of data on fatigue and fracture properties of pipeline welds. NIST has advanced material characterization capabilities and a facility for performing mechanical testing in hydrogen. Therefore, the existing data set can be extended with other welds to form a comprehensive study.

In this report, we will first provide the results of a literature review of hydrogen effects on base line pipe materials and on welded microstructures. We will focus this section on a review of hydrogen effects on steels in general, followed by a thorough review of the microstructures generated through typical welding processes on typical line pipe, and finally a review of hydrogen effects on those microstructures. We then present two specific examples of weld microstructures and their mechanical performance in hydrogen: one which shows adequate mechanical performance for hydrogen service and the other with severe degradation of properties in hydrogen. Next, we will review the codes and standards related to hydrogen and natural gas transport by pipeline, with a specific focus on highlighting gaps in the application of these codes and standards to welds. We then review 49 CFR Part 192 to assess whether hydrogen is adequately covered by existing regulations. Our approach for Phase II of this work will be described, and we will list known related work that this project will compliment.

Literature Review

Hydrogen Effects on Ferritic Steels

The degradation of mechanical properties of materials exposed to hydrogen was first recognized over a century ago when Johnson [8] observed changes in the physical properties of iron and steel exposed to hydrogen. Johnson reported significant decreases in both the fracture toughness and breaking strain, but also noted that these effects were reversible when the steels were removed from the hydrogen environment. This phenomenon, now known broadly as "hydrogen embrittlement," is generally found in most structural metals, including the ferritic steels primarily used for long-distance gas transmission pipelines.

In the time period since hydrogen embrittlement was first observed, a great deal of research has been conducted on the problem. In spite of this effort, there are many aspects of hydrogen embrittlement which are still under debate. However, the mechanism by which hydrogen enters the material is generally well-accepted [9]. Diatomic hydrogen first adsorbs on the surface of the solid, then dissociates into atomic hydrogen at the surface and chemisorbs. The hydrogen then diffuses either through the metal lattice or through grain boundaries or other defects and accumulates near internal stress centers, such as dislocations or crack tips. Figure 3 shows the range of locations where hydrogen can reside once absorbed in the material.

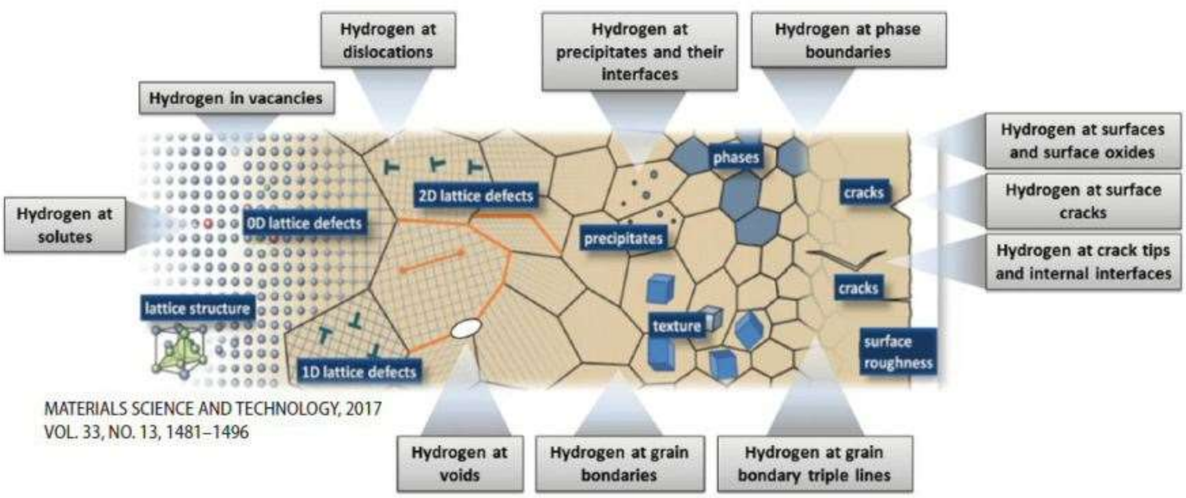

Figure 3: Various regions for hydrogen to reside once absorbed in the metal. Image from [10].

Once in the material, hydrogen can have a dramatic effect on the mechanical properties of the material. The exact influence on ferritic steels is heavily influenced by the microstructure. The high rate of hydrogen diffusion through the ferrite crystal structure renders its mechanical behavior more sensitive to the effects of microstructural features, which can act as hydrogen "traps" or sinks and have varying levels of sensitivity to hydrogen. Since ferritic steels exhibit a wide range of microstructures, some of which, like pearlite and bainite, are complex in structure, the degree of hydrogen embrittlement can cover a wide range. The degradation of by hydrogen is observed to affect a wide range of mechanical properties, including tensile properties (elongation to failure, reduction in area), fatigue crack growth rate (FCGR), and fracture toughness.

The trends in monotonic tensile tests indicate that hydrogen has little effect on the yield strength and elastic modulus of steel [11-13]. The primary effects of hydrogen observed in monotonic tensile testing are in a decrease in the elongation to failure, and a decrease in the reduction in area. A dependence on strength has been observed for both these parameters, where higher strength materials have often been observed to be more susceptible to the effects of hydrogen.

The trends in FCGR suggest an increase by a factor of 10 or more in high pressure hydrogen compared to in air. There does not appear to be a correlation between strength and degree of FCGR acceleration as observed with strength and degree of embrittlement in monotonic tensile testing [14-16]. There does appear to be some microstructure dependence on FCGR. For example, Amaro *et al.* [17] found that the FCGR increases with percentage of the microstructure consisting of polygonal ferrite.

The trends seen in fracture toughness testing in hydrogen generally follow the trends in the measurement of the threshold stress intensity factor [18]. The fracture toughness of steels in hydrogen gas is significantly reduced compared to that in air or inert environments. In general, the fracture toughness in air is at least twice as high as that in hydrogen gas at 5.5MPa or higher [19, 20], and in some cases the reduction can be quite severe, up to 90% [21]. A decrease in fracture toughness is seen in many cases as a function of increasing hydrogen gas pressure, but the slope of the trend is small [20, 22-24]. However, significant decreases in fracture toughness are seen for large increases in gas pressure for some microstructures, and a general trend is that reduced fracture toughness roughly follows the square root of pressure because of the fugacity–pressure relationship [24, 25].

The mechanism by which these reductions in mechanical performance occur is under debate. A critical review of mechanisms of hydrogen embrittlement in ferritic steels can be found in Ref. [26]; we will only briefly describe the major proposed mechanisms here: the Hydrogen Enhanced Decohesion (HEDE) mechanism, Hydrogen Enhanced Localized Plasticity (HELP), and Nano-void Coalescence (NVC) mechanism.

The HEDE model proposes that hydrogen reduces the cohesive interaction of atomic bonds, leading to decohesion of either the atomic lattice ("transgranular") or decohesion of grain boundaries ("intergranular") [27, 28]. Within the framework of HEDE, this reduction in cohesion is postulated to be related to the concentration of hydrogen. Because hydrogen is attracted to areas of high stress [29], HEDE would be most significant at areas of stress concentration, for example near cracks, planar welding flaws, or areas of high tensile residual stresses which can occur near welds. The decohesion of boundaries, whether grain boundaries or of secondary phases is one of the relatively undisputed mechanisms of hydrogen embrittlement, particularly in certain materials. Hydrogen has been clearly shown to be trapped at secondary phases, such as carbide precipitates in steels [30-32], as well as at grain boundaries [33, 34]. As hydrogen is trapped and accumulates in the boundaries of secondary phases or grain boundaries, it reduces the cohesive strength of the boundaries leading to failure. There are arguments over whether carbides, especially those rich in Ti and/or V, act as useful sinks of hydrogen that keep it away from critical areas, or whether they are critical fracture initiation sites [35]. This is particularly critical for welds, where secondary phases can form as the materials are heated during the welding process.

In the HELP mechanism, hydrogen is proposed to affect how plastic deformation manifests in the material by influencing the dislocation motion, often leading to an enhancement in the dislocation mobility as well as an increase in dislocation density [36-38]. Experimental evidence for the HELP mechanism comes primarily from *in situ* transmission electron microscopy (TEM) experiments which showed several effects on dislocations when hydrogen was introduced into the vacuum of the TEM, including increased dislocation velocity, decreased dislocation spacing, reduced cross-slip, and a reduced stacking fault energy [39-41]. More recent work has correlated brittle-appearing hydrogen-induced fracture features, such as intergranular failure or "quasi-cleavage" features, with underlying dislocation structures that could not have been generated in the absence of hydrogen [38]. Within the framework of HELP, hydrogen affects these ductile deformation processes locally and creates the conditions for failure, which may have a macroscale brittle appearance despite the ductility underlying the process [37].

In the Nanovoid Coalescence (NVC) mechanism, hydrogen stabilizes plastic damage via nanovoid formation leading to void coalescence [42, 43]. Within the framework of NVC, vacancy clusters coalesce into nano-voids which coalesce similarly to microvoids in traditional macroscale ductile fracture. Evidence for the NVC mechanism comes primarily through observation of nanovoids on fracture surfaces of fracture toughness tests, though there is some debate whether the observed fracture surfaces were created by an NVC mechanism prior to failure or relaxation processes after failure [44].

Weld and HAZ microstructures

There are several types of microstructures typical in pipeline welds and HAZs, including ferrite in various morphologies including Widmanstätten, cementite, pearlite, bainite, retained austenite, and martensite [45-47]. The type of microstructure that forms depends on the welding process used, the composition of the metal being welded, the composition (and presence of) the welding consumable, the heat input, and the cooling rate during the welding process [47]. Ferrite-pearlite microstructures are common in pipeline welds and consist of alternating bands of ferrite and pearlite. Ferrite is a relatively ductile phase, though its condition depends on the processing conditions, while pearlite is a combination of ferrite and cementite that is stronger and more brittle. The presence of ferrite in the microstructure can help to reduce the susceptibility of the weld to hydrogen-induced cracking. Bainite microstructures are characterized by a fine, needle-like structure and are formed when the metal is cooled rapidly during the welding process. This microstructure is stronger than ferrite-pearlite microstructures but may be more susceptible to hydrogen embrittlement. Martensite microstructures are very hard and strong but are also very brittle. They are formed when the metal is cooled very rapidly during the welding process, such as in a quenching process. Understanding and managing the formation of these microstructures is crucial to ensuring the long-term integrity and safety of pipeline systems.

The microstructure of the HAZ depends on the thermal cycling that occurs due to the weld, defined by the maximum temperature and cooling rate [48]. The relationship between the thermal cycling and HAZ microstructure is shown in Figure 4. During the welding process, the base metal is heated through different phases in the iron-carbide diagram, depending on the heat input and the carbon content of the base metal. Note that the carbon distribution can change during the welding process due to carbon diffusing from heating, and this can further impact the final microstructure. The base metal closest to the weld is heated to temperatures above the upper critical temperature (AC_3) and undergoes complete recrystallization from ferrite to austenite during the weld procedure; the cooling rate then determines the grain size. Of this section, the region closest to the weld fusion line experiences sufficiently high temperatures for sufficient time for grain growth to occur after recrystallization, resulting in a Coarse-Grained HAZ (CG-HAZ). Further from the weld fusion line is an area which has undergone recrystallization but no grain growth, resulting in grain-refinement relative to the original grain size, the Fine-Grained HAZ (FG-HAZ). The next region away from the weld fusion line experiences temperatures lower than AC_3 but above the lower critical temperature AC_1, resulting in only partial recrystallization, and is known as the Inter-Critical HAZ (IC-HAZ). Base material further from the fusion line, in an area known as the over-tempering zone, is not heated through any phase transformations on the iron-carbide diagram, however sufficient tempering can occur to result in softening of the material.

The nature of the CG-HAZ, FG-HAZ, and IC-HAZ is dependent on the peak temperature as well as the cooling rate, which determines the dwell time within the austenite zone. The cooling rate is often referred to in terms of the time required for the metal to cool between a specified temperature interval. Most common is the interval between 800C and 500C, termed $\Delta t_{8/5}$. The $\Delta t_{8/5}$ depends on the heat input during the welding process, the chemistry of the pipe, the distance from the weld, and the wall thickness of the pipe. Proper control of the welding process and the cooling rate of the weld can help to minimize the effects of the inter-critical weld region on the mechanical properties of the metal. Pre-heat and post-weld heat treatment procedures can help control the final microstructure. The peak temperature greatly affects the austenitizing and its grain size, thereby affecting the phase transition during cooling process. Accelerating cooling with cooling time $\Delta t_{8/5}$ of 8 s has been shown in the field for in-service welding X70 pipeline to control microstructures and improve toughness. The cooling rate is one of the important parameters in coarse grain heat affected zone of pipeline steels.

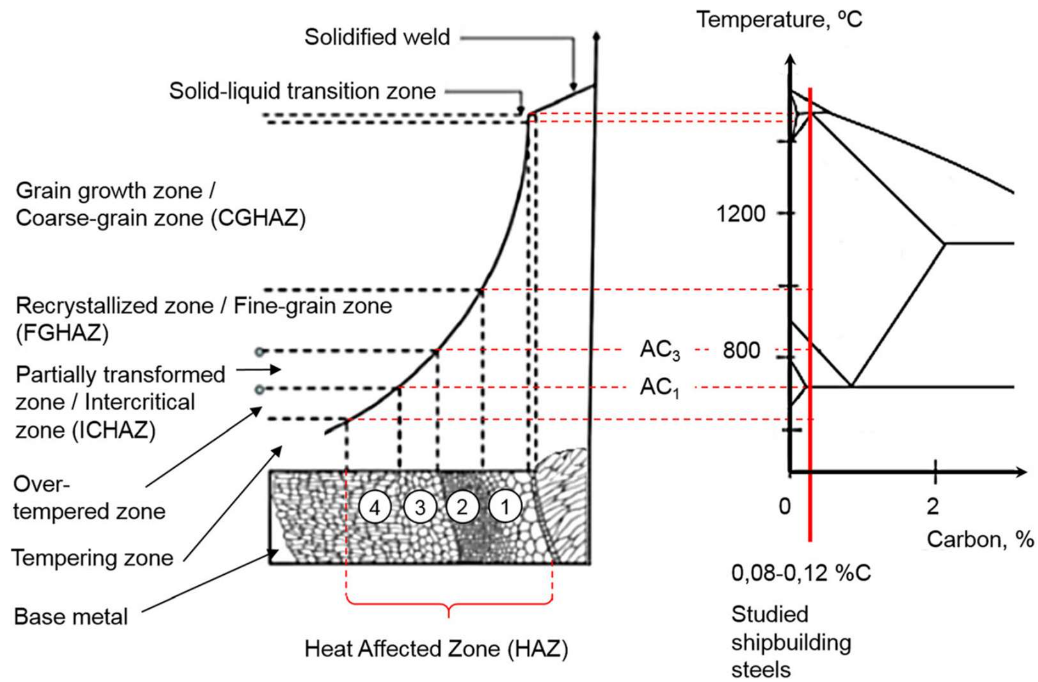

Figure 4: Relationship between the HAZ microstructure and iron-carbide diagram. Image taken from [48].

Martensite is a hard, brittle, highly-stressed, metastable phase that forms in steel when it is rapidly cooled from a high temperature. In the HAZ, martensite forms during rapid cooling which occurs closest to the weld in the CG-HAZ and FG-HAZ. Austenite is a high-temperature phase of steel that is stable above the critical temperature. In the HAZ, retained austenite can form due to the high temperatures and fast cooling rates caused by the welding process. Martensite-Austenite (M-A) constituents are islands comprised of a mixture of martensite and retained austenite [49]. Bainite forms in steel when it is cooled at an intermediate rate between the rates required for martensite and pearlite. In the HAZ, bainite can form due to the intermediate cooling rates in the IC-HAZ.

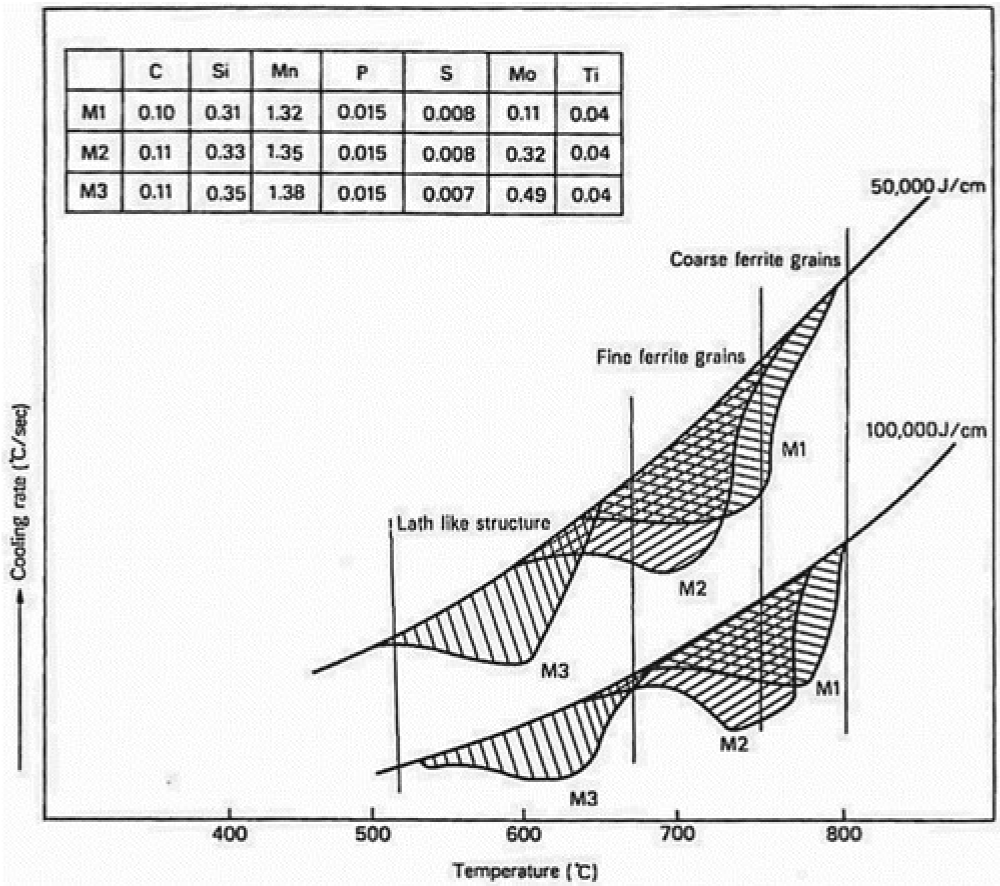

Figure 5: The complex relationship between temperature, cooling rate, and composition and the type of grains formed in pipeline steel. Image from [50].

The microstructure of the weld and HAZ depends on the composition of the base metal [51], as well as the composition of the filler material. Zhu et al. found an increase in Charpy energy and crack tip opening displacement (CTOD) value with an increase in Ti/N ratio. It was found that Ti-Nb-V precipitates in the CGHAZ region produced fine austenite grains [52]. Ni has been observed to restrict the grain size in the weld metal of an X80 pipe with SMAW welds, while Mn was observed to promote the formation of acicular ferrite [53]. Nb content in the base material has been shown to limit the grain size of the CGHAZ [54].

The microstructure gradient across the weld, HAZ, and base metal have complicated the studies of mechanical properties, as it is difficult to isolate single microstructures in, for example, tensile or Charpy specimens. Weld thermal simulations, which is the process of applying precise heating and cooling rates to larger areas of material have been used to generate microstructures observed in HAZ thermal gradients, but on a size scale which lends itself better to mechanical testing. Figure 6 shows an example of maximum temperature and cooling rates as well as the microstructures generated.

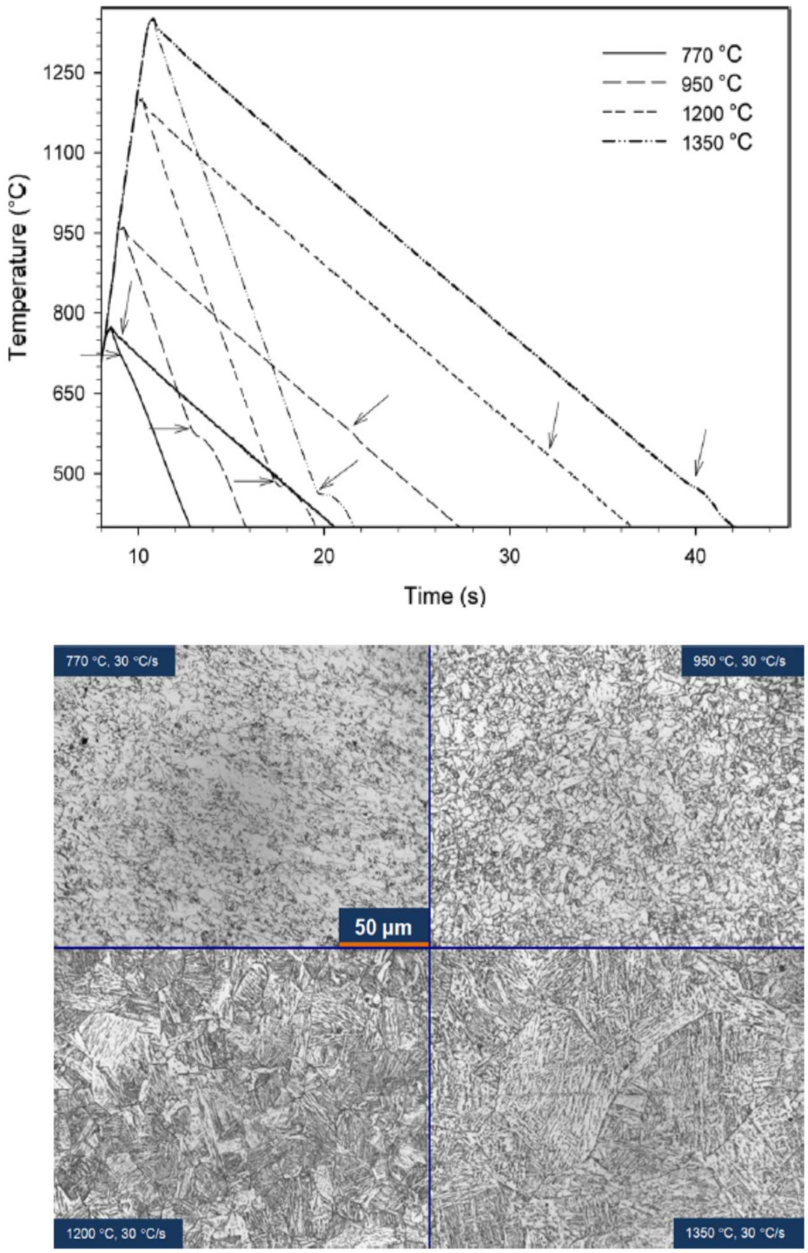

Figure 6: Simulated weld heating and cooling (top) which generated difference microstructures.

Repeated thermal cycles imposed by the combined multi-pass girth welding process complicates welding microstructures even further, as depicted in Figure 7. For example, during the second weld pass, the CGHAZ is reheated to an intercritical temperature to form a new zone, ICCGHAZ. In this region the coarse austenite structure transforms to bainite or martensite and is then reheated to a coarsened bainitic structure with islands of high carbon austenite. These islands are referred to as "retained austenite and martensite consitutuents" or M-A. The number of M-A islands in the grain-coarsening region of an X80 pipeline steel increases with increasing thermal input, which in turn increases the cooling rate.

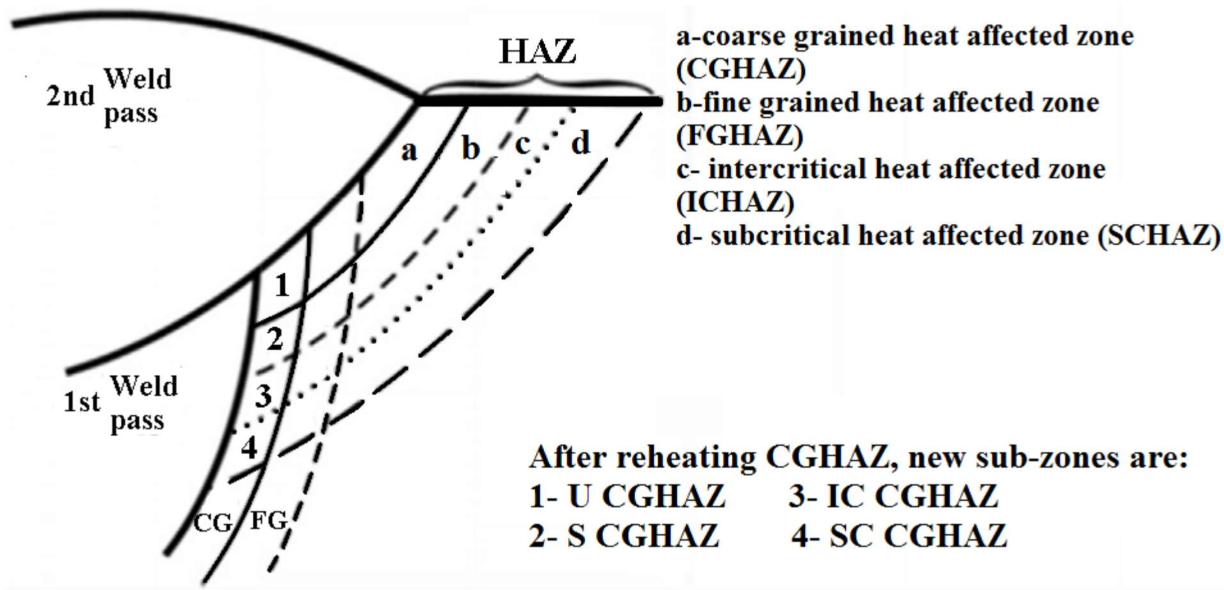

Figure 7: Diagram of multi-pass welding, showing how complex microstructures are generated once CG-HAZ, IC-HAZ, and FG-HAZ zones are reheated. Image taken from [49].

Microstructural effect on hydrogen susceptibility

A microstructure effect on the hydrogen susceptibility can be observed in monotonic tensile testing. For example, Zhang et al. measured the relative reduction in area during tensile testing of an X80 pipeline steel base and HAZ [55]. Relative to the base metal, the susceptibility of the

HAZ areas to hydrogen go in order of IC-HAZ, FG-HAZ, to CG-HAZ, with the CG-HAZ being the most susceptible to degradation by hydrogen.

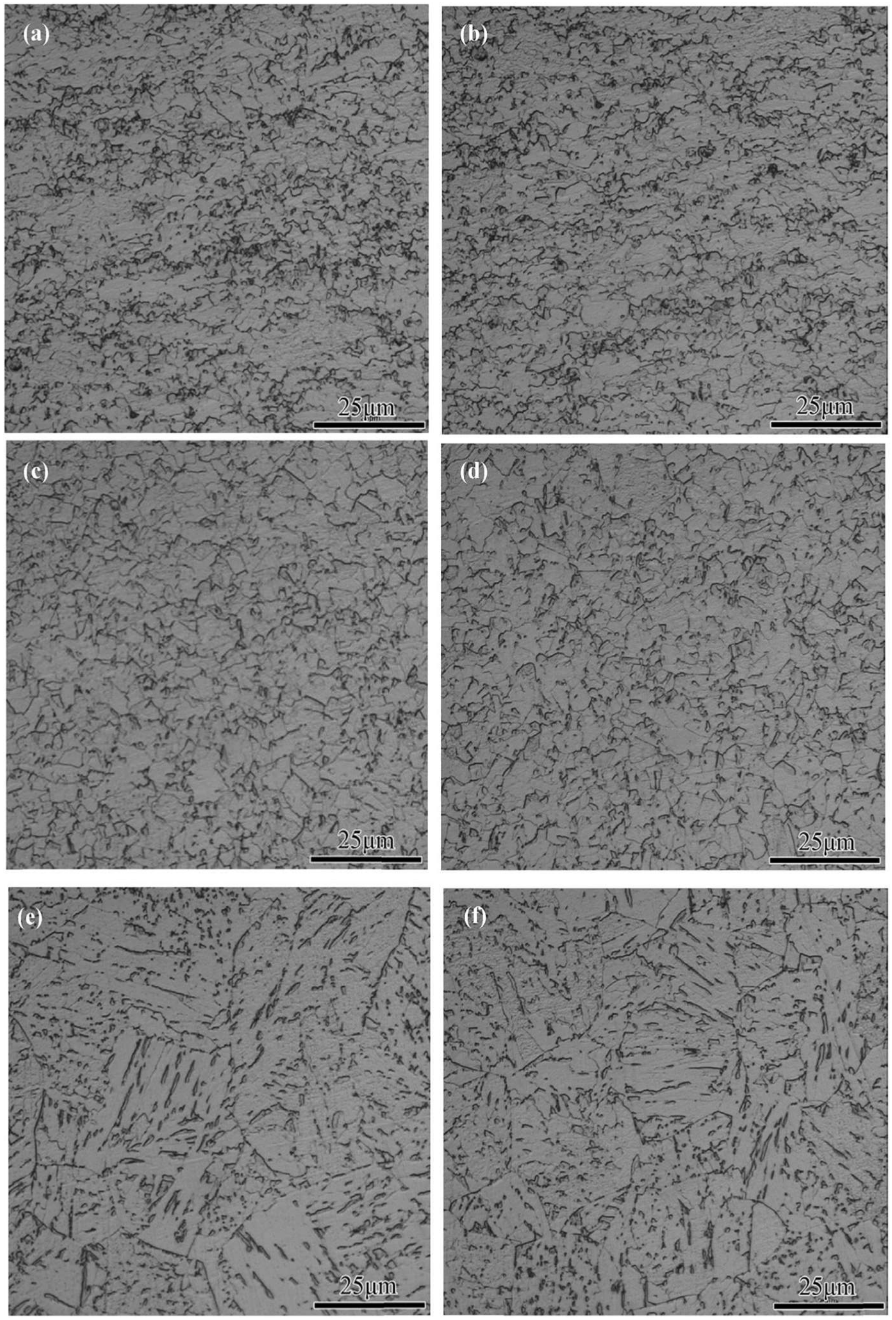

Figure 8: a) Simulated ICHAZ, b) ICHAZ in welded joint, c) simulated FGHAZ, d) FGHAZ in welded joint, e) simulated CGHAZ, f) CGHAZ in welded joint. Image from Ref. [55].

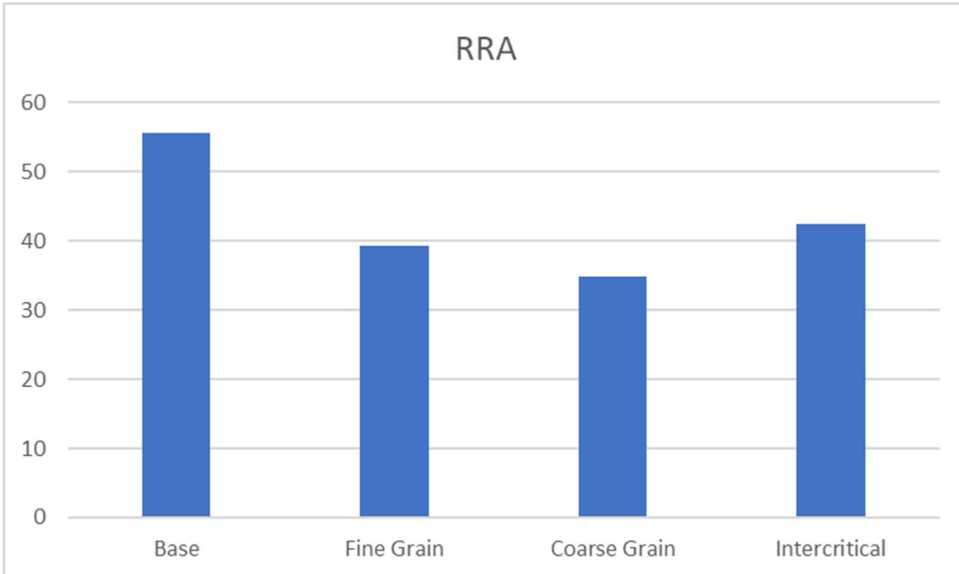

Figure 9: Relative reduction in area (RA_H - RA_{air})/(RA_{air}) for base metal and different HAZ regions. Data from [55].

In terms of FCGR, some evidence suggests differences in hydrogen susceptibilities for different microstructures. For example, in Figure 10: Fatigue crack growth rates for various microstructures of steel. Figure reproduce from [26].Figure 10, the material with purely polygonal ferrite microstructure was shown to have the fastest FCGR, while microstructures consisting partially of acicular ferrite, bainite, or pearlite had relatively lower FCGR in hydrogen. Pearlite showed the lowest susceptibility to hydrogen in terms of FCGR, though some measurements have shown a directional dependence, where cracks running parallel to pearlite bands are highly susceptible to hydrogen while cracking perpendicular to the pearlite bands show lower susceptibility.

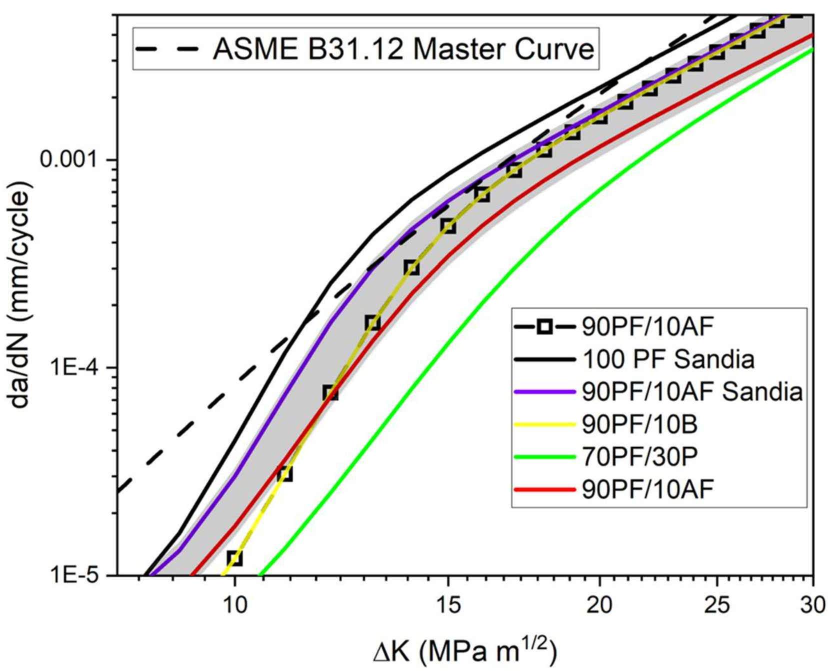

Figure 10: Fatigue crack growth rates for various microstructures of steel. Figure reproduce from [26].

Hydrogen has been observed to have a severe effect on the fracture toughness of steels, with a significantly larger effect in the HAZ [56]. In general, it has been observed that hydrogen reduced the fracture toughness by at least a factor of two when the gas pressure is 5.5 MPa or higher. On electro-chemically charged specimens by Alvarez *et al.*, a ferrite-pearlite microstructure was observed to have a small decrease in fracture toughness in hydrogen, while a large decrease was observed for a ferrite-martensite [57]. Like FCGR, fracture toughness decreases in hydrogen gas to not appear correlated to yield strength, however the fact that a range of microstructures can lead to similar yield strengths but different susceptibility to hydrogen complicates this statement [19, 23].

In general, the current evidence strongly suggests either a microstructural dependence on hydrogen susceptibility, or at least that some microstructures are particularly susceptible or resistant to hydrogen. However, more systematic studies need to be performed to fully elucidate such a correlation, and to link that correlation to welding processes. For example, although the addition of Nb has been shown to reduce cold cracking during welding processes, it remains to be seen whether the reduction in CGHAZ grain size leads to an improved performance, in terms of tensile properties, FCGR, and fracture toughness, in hydrogen gas.

In the following, we will show two case studies of steel pipeline weld microstructures and their performance in hydrogen. In the first example, the base metal shows a particular resistance to degradation by hydrogen, but the susceptibility of the HAZ microstructure is severe. In this example, the loss in toughness due to hydrogen at the CGHAZ is sufficient to disqualify the weld for hydrogen service. In the second example, a large decrease in fracture toughness is observed for both the weld and HAZ in hydrogen, however the HAZ microstructure retained sufficient toughness in hydrogen to still qualify for hydrogen service. Additionally, the FCGR was slower in this material’s weld compared to the base metal.

Example case 1:

NIST has tested the fracture toughness of base, weld, and HAZ material for a girth weld in a seamless, quenched-and-tempered line pipe, of EN10216-3 P690QL2 grade. The base metal had a yield strength of 754 MPa and ultimate tensile strength of 822 MPa. In air, the elongation to failure of the base material was 19%. An optical macrograph is shown in Figure 11~~Figure 11~~. Note that the weld is composed of a series of beads, resulting in a fusion that is nearly vertical to the through-thickness of the weld in many areas. The hardness scan across the base metal, HAZ, and weld metal is shown in Figure 12~~Figure 12~~. Note that the hardness of the base metal, HAZ, and weld all exceed the hardness limit in ASME B31.12 of 235 Vickers. The hardness of the base metal does not, however, exceed the hardness limit of 280 Vickers in 49 CFR Part 192.

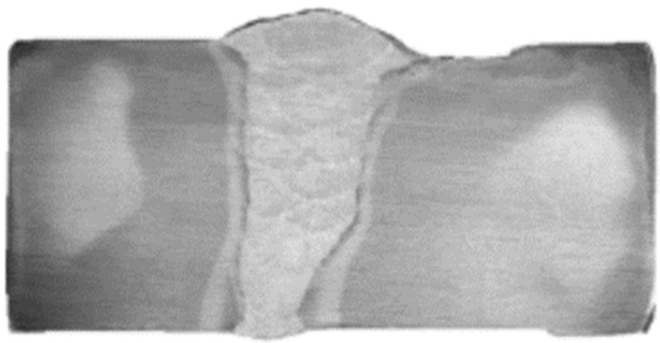

Figure 11: Optical macrograph of weld in example case #1.

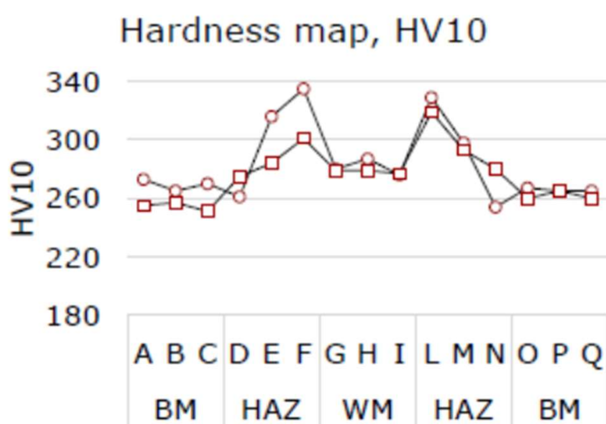

Figure 12: Hardness line scans across the base metal (BM), HAZ, and weld metal (WM) for the weld in example case #1.

The load versus crack mouth opening displacement (CMOD) data from the fracture toughness tests of the base metal in 20 MPa (2900 psi) hydrogen gas, the HAZ in 200 bar hydrogen gas, and the HAZ in air are shown in Figure 13~~Figure 13~~. Due to the expected high toughness of the base metal in air, this was not tested. The base metal had a maximum load of approximately 75 kN at a CMOD of 0.75 mm. A lower maximum load was observed for the HAZ tested in hydrogen gas compared to the base metal tested in hydrogen gas. The HAZ material tested in air had a higher load than either material tested in hydrogen of approximately 90 kN at a CMOD of 1.1 mm. The HAZ tests in hydrogen gas show a noticeable drop in the load vs. CMOD data beyond a CMOD of approximately 0.5 mm, where the load decreased significantly and the CMOD increased. This is indicative of a tearing instability.

The J-R curves indicate a high toughness for the HAZ in air. The base metal in hydrogen showed a somewhat decreased toughness. For the HAZ, two tests (C01 and C03) showed J-R curves which followed that of the base metal until a crack extension of approximately 1 mm, before unstable crack extension was observed.

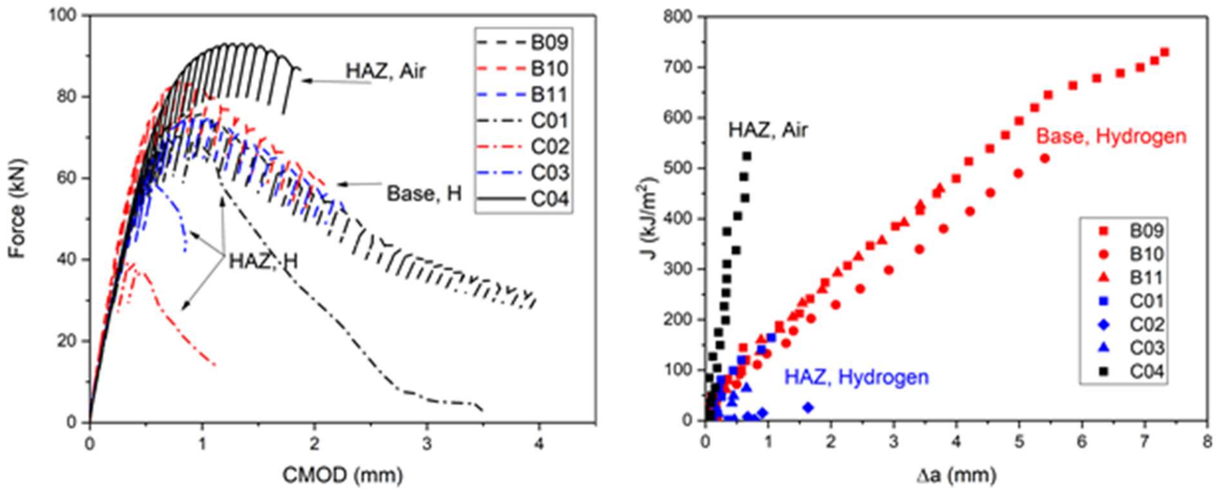

Figure 13: Force vs CMOD relationship for the base material in hydrogen, HAZ in hydrogen, and HAZ in air, and b) the associated J-R curves.

The HAZ specimens displayed signs of tearing instabilities during the test. It is important to consider the presence of tearing instabilities when assessing the performance of the material. This is especially true for the HAZ specimens, which could have a crack path which initiates in a tough base material followed by a tearing instability through HAZ material. The other HAZ specimen tested in hydrogen (C02) showed very low J capacity before tearing instabilities were observed. This is indicative of a very low toughness of the HAZ in hydrogen.

Optical microscopy of the crack path for specimen C03 shows the crack initiated in a fine-grained HAZ while the tearing instability occurred in the coarse-grained HAZ (see Figure 14). SEM images of the fracture surfaces for the base metal and the HAZ specimen C01 are shown in Figure 15. The fracture surface of the main crack appears to have deviated from the initial crack plane by as much as 2 mm, which is likely the path taken from initiation to tearing instability. The SEM images indicate intergranular failure, suggesting failure along prior austenite grain boundaries.

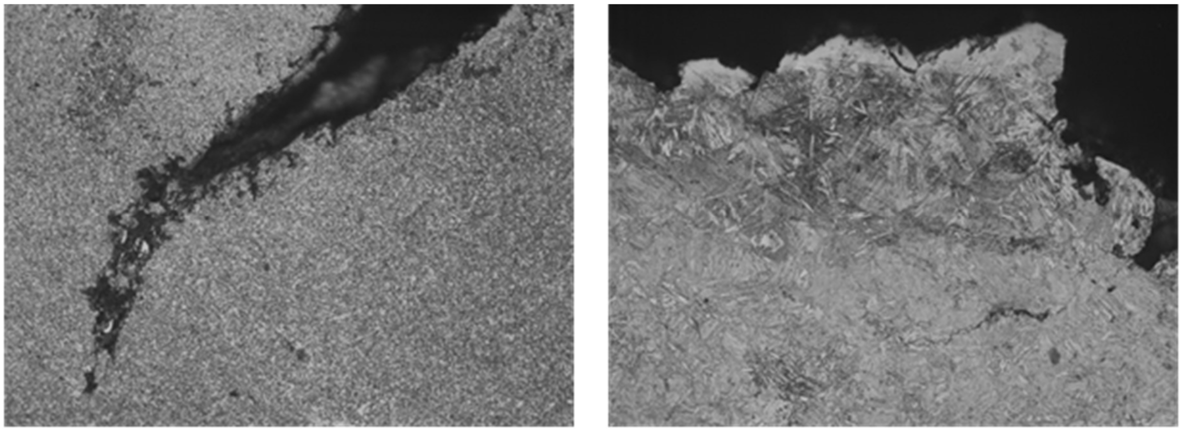

Figure 14: Crack growth through fine-grained HAZ (left), through which the specimen was able to hold load, and crack path through the coarse-grained HAZ (right), which was indicated by a fracture instability in the Force vs. CMOD curve.

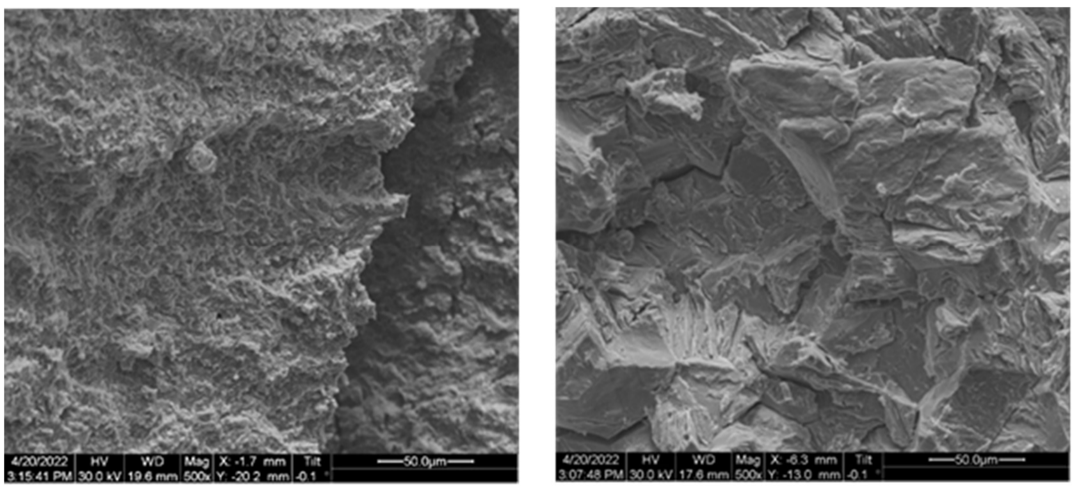

Figure 15: SEM images of the fracture surface at the crack initiation (left) and at the point of fracture instability (right).

Example case 2:

NIST measured a commercially-obtained X70 pipe steel of interest for use in blended natural gas/hydrogen service. The macrostructure Figure 16 (top) shows long prior austenite grain structures radiating from the root to the surface of the bead consisting of fine Widmanstätten ferrite plates with allotriomorphic ferrite along the prior austenite grain boundaries. On both sides of both weld beads, there are wide (~2 mm) heat affected zones (HAZs). Only a narrow (< 100 µm) CGHAZ is observed near the fusion line, shown in Figure 16 (bottom).

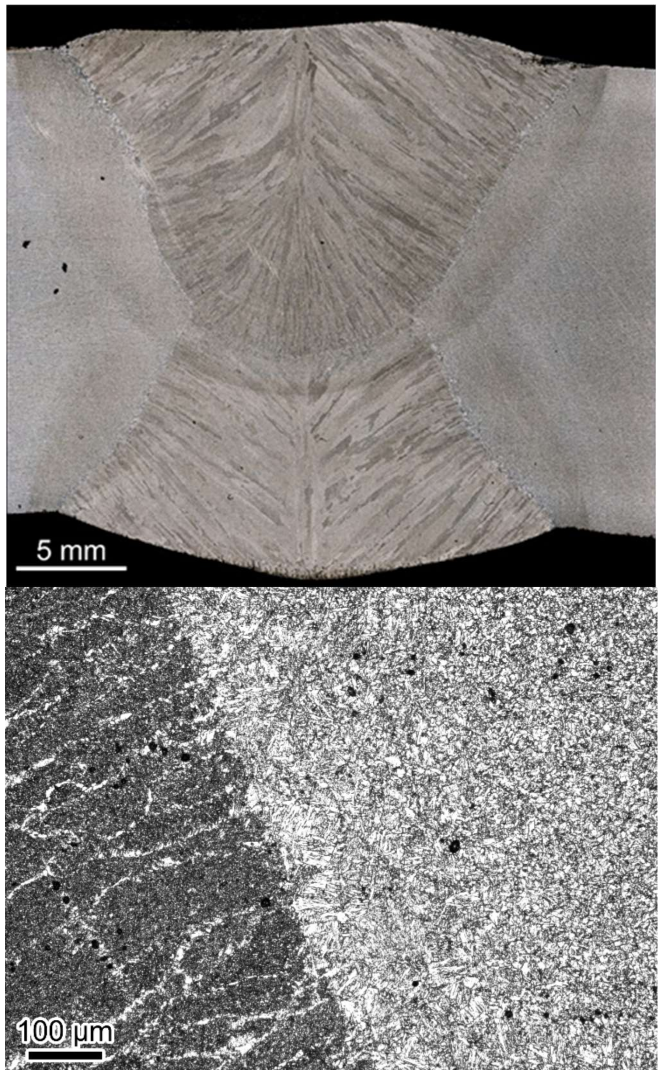

Figure 16: Optical macrograph (top) and micrograph (bottom) showing the weld, HAZ, and base metal of an X70 steel.

Fracture toughness (J_{IC}) tests were run according to ASTM E1820 on side-grooved compact tension (CT) specimens in air and in 10 MPa hydrogen gas [21]. Specimens were machined from the pipe wall according to the ASTM E1820 standard with a nominal width (W) of 40.6 mm. Samples were oriented with the crack direction in the rolling direction for the base metal and with the crack to the side of the weld beads to capture the heat affected zone (HAZ), as well as weld metal, for the seam weld metal. The fracture toughness was determined from J-R curves, which were measured using a crack mouth opening displacement (CMOD) sensor and the compliance method to determine crack extension.

The load versus CMOD data from the fracture toughness tests of the base metal in air, the base metal in 10 MPa hydrogen gas, and the HAZ in 10 MPa hydrogen gas are shown in Figure 17. A drop in maximum load is observed for both the base metal and the weld tested in hydrogen gas compared to the base metal in air. Further, the CMOD at which the maximum load is reached is decreased due to hydrogen, from approximately 2.45 mm in air to approximately 0.9 mm in hydrogen. For the two tests in hydrogen gas, the CMOD at which the maximum load is reached is roughly the same, however the maximum load was higher for the base metal compared to the HAZ (51 vs 38 kN).

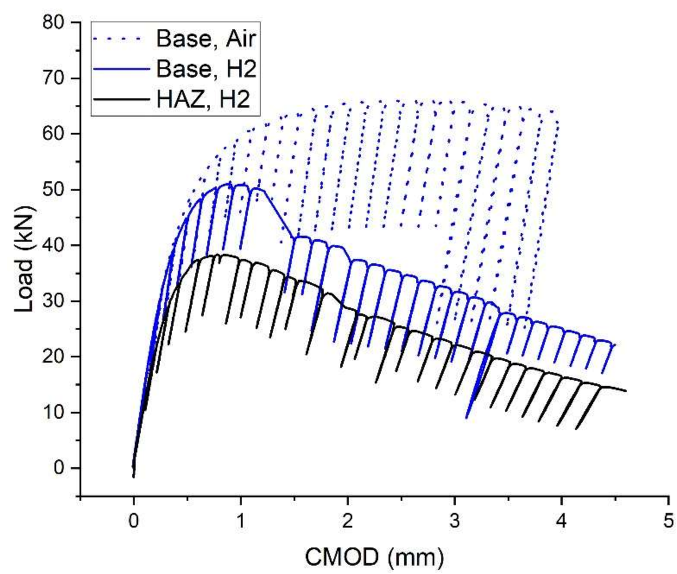

Figure 17: Load - CMOD curve for the base metal test in air, and the base and HAZ test in hydrogen.

A noticeable step in the load vs. CMOD data was observed for the base metal tested in hydrogen, where the load decreased significantly, and the CMOD increased starting at ~~a CMOD of~~ approximately 1.2 mm. This may be due to delamination, which was observed in both the base metal and HAZ fracture surfaces for the specimens tested in hydrogen gas, shown in Figure 18**Error! Reference source not found.**. A delamination in this case is a secondary crack which is perpendicular to the primary crack plane. A similar step was observed at a CMOD of approximately 1.75 mm for the HAZ material, though the magnitude of the load drop was significantly smaller than for the base metal. However, the large number of complicated features, including multiple delaminations and evidence of crack arrest events, on the base metal in H_2 surfaces make it difficult to ascertain that the delaminations are the cause, or sole cause, of the load drops.

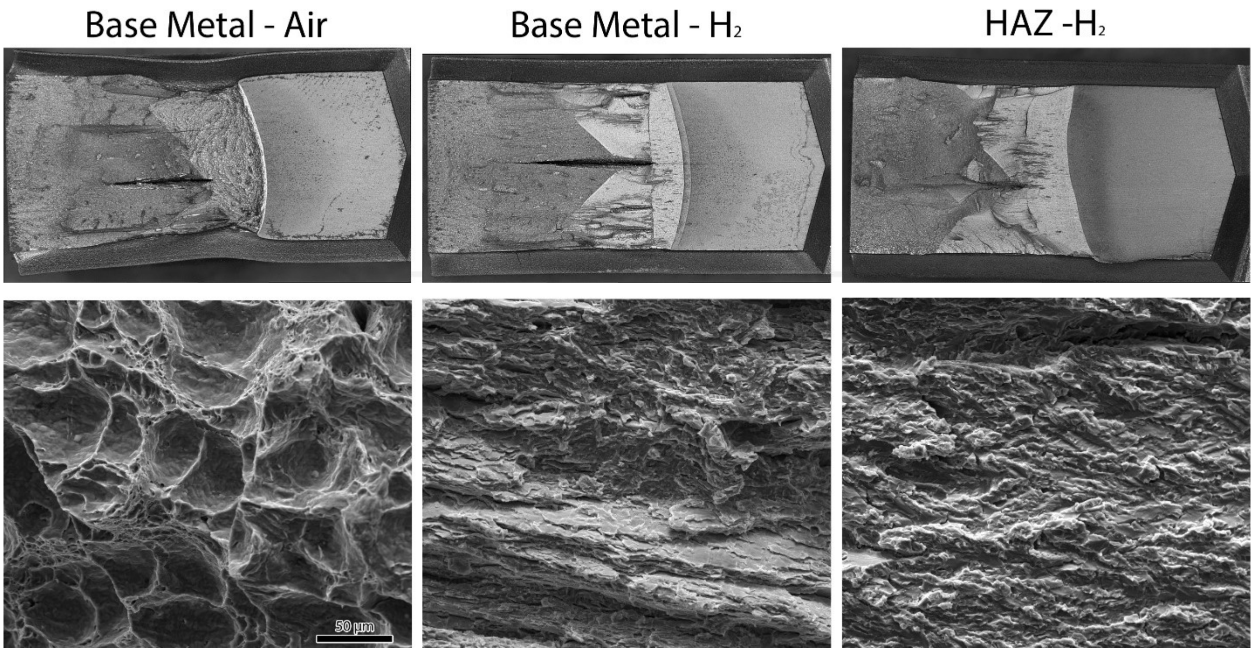

Figure 18: Optical (top row) and SEM (bottom row) images of fracture toughness specimens.

Figure 19 shows a representative J-R curves for the base metal in air, the base metal in 10 MPa hydrogen gas, and the HAZ in 10 MPa hydrogen gas. The J_{IC} under each condition is compared in the bar chart in Figure 20. The base metal in air clearly has a significantly higher J_{IC} compared to either material in 10 MPa hydrogen. The HAZ and base metal J_{IC} in 10 MPa hydrogen are similar, though the base metal has a slightly higher J_{IC}. Consistent with fractography, the high in-air J_{IC} indicates a huge amount of plastic deformation near the crack tip without associated crack growth, while the hydrogen-embrittled material displays significantly less plastic deformation as the crack extends.

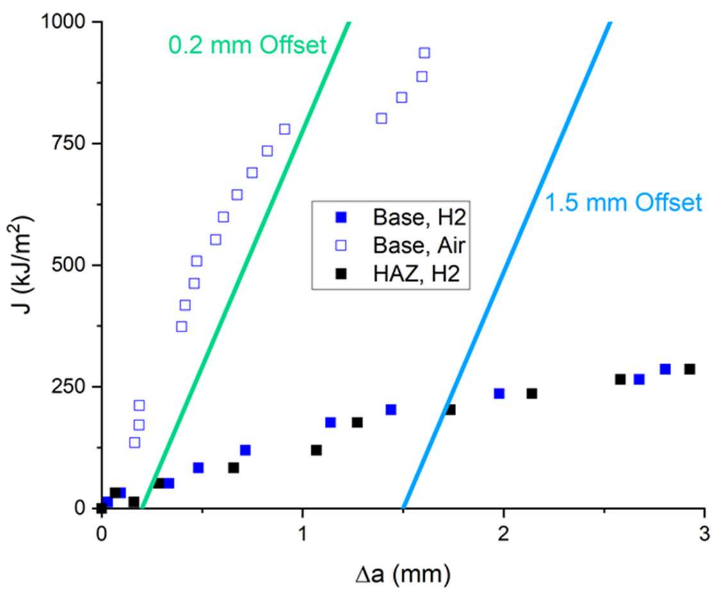

Figure 19: J-Δa curves for base metal in air and in hydrogen and of HAZ material in hydrogen. Image from [21].

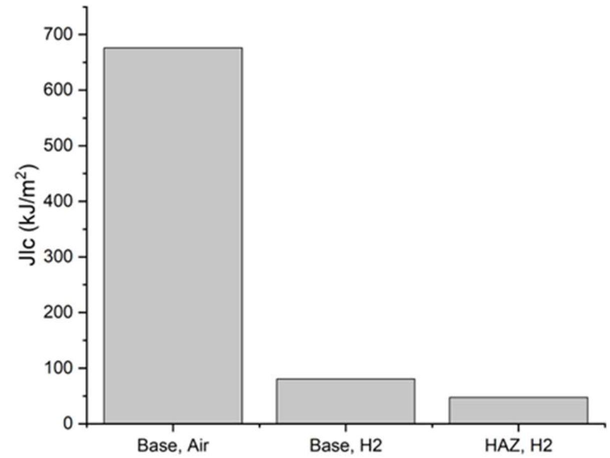

Figure 20: Fracture toughness values of base metal in air and in hydrogen gas, and of HAZ material in hydrogen gas. Image from [21].

Fatigue crack growth rate (FCGR) tests were run on CT specimens without side grooves in 10 MPa hydrogen gas from the base metal (3 samples) and the weld (3 samples). The base metal fatigue samples were cut similarly to the fracture toughness samples, with the cracking direction following the rolling direction; the weld samples were cut so that the crack goes down the center of the two weld beads, also parallel to the rolling direction. Pre-cracking was performed in air at room temperature with a load ratio, R = 0.1, and loading frequency of 15 Hz. These samples were run simultaneously in a chain, see [58] for details on the experimental setup, such that they all experienced the identical gaseous environment during mechanical loading. Fatigue tests were conducted with R = 0.5 at a loading frequency of 1 Hz.

Figure 21 shows the FCGR for the base and weld materials in hydrogen as a function of ΔK, the change in crack tip stress intensity factor. The plot also shows the "Master Curve", as outlined in the Boiler and Pressure Vessels Code Section VIII [59] and described in Ref. [4]. In general, for both the weld and base material, the FCGR increases with ΔK, spanning from ~10^{-5} mm/cycle when ΔK is ~10 MPa·$m^{1/2}$ to ~10^{-3} mm/cycle when ΔK is ~20 MPa·$m^{1/2}$. At ΔK of approximately 12 MPa·$m^{1/2}$, there is a clear "knee" in the data where the log-log plot is observed to transition ~~from~~ to a smaller slope. For all measured ΔK, the FCGR for both the weld and base metal is below the Master Curve.

In general, the FCGR is slower in the weld material compared to the base metal. There is also a larger spread in measured FCGR between specimens for the weld material compared to the base metal. Both effects are likely due to residual stresses within the weld region.

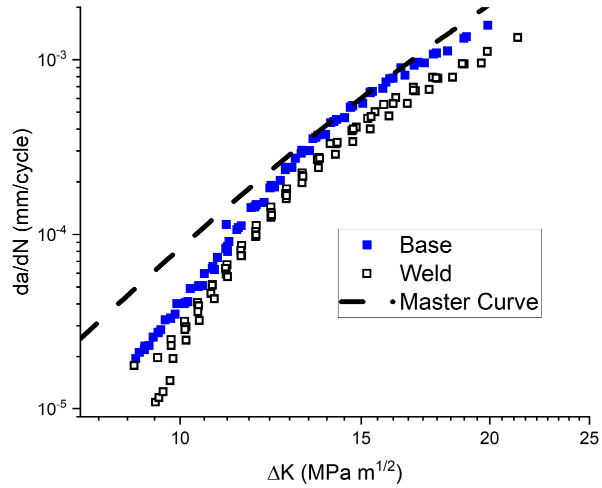

Figure 21: FCGR curves of base and weld metal and the "Master Curve" from [59]. Image from [21]

Codes and Standards Review

ASME B31.12

The relevant section from B31.12 for qualifying steels (including welds) for hydrogen service is ASME B31.12 PL-3.7.1. Within PL-3.7.1 there are three options for qualifying steels when designing for *Fracture Control and Arrest*. The first is a Prescriptive Design Method, which limits operating design pressure to 3000 psi (21 MPa) and 40% of specified minimum yield strength (SMYS). If the pipeline is designed to operate at a hoop stress under 40% of SMYS, then engineering and design for fracture control and arrest is not necessary. Secondly, one could use PL-3.7.1(b)(1) Option A (requiring Charpy or DWTT of base material(s) and weld(s)/HAZ(s)) if one is willing to use the Material Performance Factors listed in Table IX-5A.

(1) Option A (Prescriptive Design Method). The following requirements apply:

(-a) Brittle Fracture Control. To ensure that the pipe has adequate ductility, fracture toughness testing shall be performed in accordance with the testing procedures of Annex G of API 5L. These can be applied providing test specimens meet the minimum sizes given in Table 22 of API 5L. Toughness testing for brittle fracture control is not required for pipe sizes under 114.3 mm (4.5 in.). The test temperature shall be the colder of 0°C (32°F) or the lowest expected metal temperature during service or during pressure testing, if the latter is performed with air or gas, having regard to past recorded temperature data and possible effects of lower air and ground temperatures. The average shear value of the fracture appearance of three Charpy specimens from each heat shall not be less than 80% for full-thickness Charpy specimens, 85% for reduced-size Charpy specimens, or 40% for drop weight tear testing specimens.

(-b) Ductile Fracture Arrest. To ensure that the pipeline has adequate toughness to arrest a ductile fracture, the pipe shall be tested in accordance with Annex G of API 5L. This can be applied providing test specimens meet the minimum sizes given in Table 22 of API 5L. Toughness testing for ductile fracture control is not required for pipe sizes under 114.3 mm (4.5 in.). The test temperature shall be the colder of 0°C (32°F) or the lowest expected metal temperature during service. The average of the Charpy energy values from each heat shall meet or exceed the requirements specified by the following equation:

$$CVN = 0.008\,(RT)^{0.039}{\sigma_h}^2$$

where *CVN = full-size specimen CVN energy, ft-lb, R = radius of pipe, in. T = nominal pipe wall thickness, in., σ_h = hoop stress due to design pressure, ksi*

(-c) Pipe Strength. Maximum ultimate tensile strength of the pipe shall not exceed 100 ksi (690 MPa).

(-d) Weld Metal Strength. Maximum ultimate tensile strength of the weld metal shall not exceed 100 ksi (690 MPa).

(-e) Yield Strength. Minimum specified yield strength shall not exceed 70 ksi (483 MPa).

(-f) Charpy Tests. Weld procedure shall be qualified by Charpy tests. Three specimens from weld metal and three specimens from HAZ shall be tested at test temperature specified in (b)(1)(-b) above. Minimum Charpy energy per specimen fracture area of each specimen shall meet the following criteria:

(-1) 20 ft-lb for full-size CVN specimens or 161 ft-lb/in.^{2} for subsize CVN specimens for pipe not exceeding 56 in. outside diameter

(-2) 30 ft-lb for full-size CVN specimens or 242 ft-lb/in.^{2} for subsize CVN specimens for pipe outside diameter >56 in.

The Material Performance Factors listed in Table IX-5A are shown in Figure 22.

Table IX-5A Carbon Steel Pipeline Materials Performance Factor, H_f

Specified Min. Strength, ksi		System Design Pressure, psig						
Tensile	Yield	≤1,000	2,000	2,200	2,400	2,600	2,800	3,000
66 and under	≤52	1.0	1.0	0.954	0.910	0.880	0.840	0.780
Over 66 through 75	≤60	0.874	0.874	0.834	0.796	0.770	0.734	0.682
Over 75 through 82	≤70	0.776	0.776	0.742	0.706	0.684	0.652	0.606
Over 82 through 90	≤80	0.694	0.694	0.662	0.632	0.610	0.584	0.542

GENERAL NOTES:

(a) Tables IX-5A, IX-5B, and IX-5C are for use in designing carbon steel, low, and intermediate alloy piping and pipeline systems that will have a design temperature within the hydrogen embrittlement range of the selected material [recommended lowest service temperature up to 300°F (150°C)]. If the system design temperature is out of this range, use the design allowable stresses from Table IX-1A for piping or the specified minimum yield strength for pipelines from Table IX-1B.

(b) Table IX-5A was developed for pipeline systems and as such the design factors are based on the specified minimum yield strength of the material ranges shown.

(c) Design factors may be calculated by interpolation between pressures shown in the tables.

(d) For materials not covered by Tables IX-5A, IX-5B, and IX-5C, use the allowable stresses in Table IX-1A.

Figure 22: Material Performance Factors from ASME B31.12.

The weld qualification procedure is directly addressed in Option A, part f, which specifies a minimum Charpy energy of 20 ft-lb for pipelines with outside diameter not exceeding 56 in. and 30 ft-lb for a pipe diameter greater than 56 in. **These minimum Charpy requirements for the welds and HAZs are significantly less than the minimum Charpy requirements for the base metal,** for all but small diameter pipes with very thick walls. As an example, Figure 23 shows a contour plot of minimum CVN according to the equation in Option A, part b, for a range of pipe radii and wall thicknesses, assuming a service pressure of 3,000 psi.

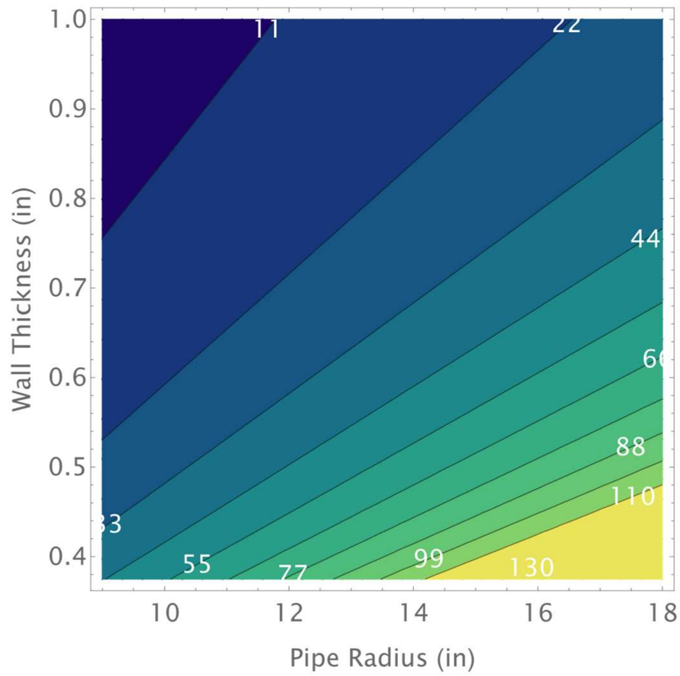

Figure 23: Contour plot of minimum Charpy energy for the pipeline base metal according to Option A, part b. Note that the minimum Charpy energy for the base metal significantly exceeds the minimum Charpy energy for the weld and HAZ according to Option A, part f.

Thirdly, one could use PL-3.7.1(b)(1) Option B (requiring Charpy or DWTT of base material(s) and weld(s)/HAZ(s) as well as a full design fatigue life analysis per ASTM BPVC.VIII.3 Article KD-10) if one is needing to reduce the effect of the Material Performance Factor for materials having SMYS> 52 ksi.

> *(2) Option B (Performance-Based Design Method). The following requirements apply: (-a) The pipe and weld material shall be qualified for adequate resistance to fracture in hydrogen gas at or above the design pressure and at ambient temperature using the applicable rules provided in Article KD-10 of ASME BPVC, Section VIII, Division 3, except as shown below.*
>
> > *(-1) The purpose of this test is to qualify the construction material by testing three heats of the material. The threshold stress intensity values, KIH, shall be obtained from the thickest section from each heat of the material and heat treatment. The test specimens shall be in the final heat-treated condition (if applicable) to be used in pipe manufacturing. A set of three specimens shall be tested from each of the following locations: the base metal, the weld metal, and the HAZ of welded joints, welded with the same qualified WPS as intended for the piping manufacturing. A change in the welding procedure requires retesting of welded joints (weld metal and HAZ). The test specimens shall be in the TL direction. If TL specimens cannot be obtained from the weld metal and the HAZ, then LT specimens may be used. The*

values of KIH shall be obtained by use of the test method described in KD-1040. The lowest measured value of KIH shall be used in the pipeline design analysis.

(-2) When using Option B, the material performance factor, H_f, used in (a) shall be 1.0.

Note that KD-1040 requires that K_{IH} values be determined for base material, weld material, and HAZ (in triplicate), by use of ASTM E1681. The application of a testing standard based upon linear elastic fracture mechanics to materials exhibiting large scale plasticity, such as pipeline steel which more appropriately falls within elastic-plastic fracture mechanics regime, has stunted the application of the B31.12 code in its ability to provide usefulness in practice. That is, when following ASTM E1681 specimen sizing requirements, one will note that the average thickness required of test specimens to meet the validity criteria for K_{IH} values is well over 1 in.

Work by Sandia National Labs (and their larger working group) has indicated that the fracture toughness values attained by use of ASTM E1820 (also termed initiation threshold from rising-displacement tests) in hydrogen provide a lower-bound estimate of the KIH values estimated by use of ASTM E1681 (also termed constant displacement tests) [60]. **Their work is currently being reviewed as part of a potential code change within the BPVC to modify Article KD-1040 to allow for the use of either ASTM E1681 or ASTM E1820 when determining a materials crack threshold resistance in hydrogen environments.** The ASME BPVC committee's primary focus is on pressure vessel applications. The ductility of an average API pipeline material is often greater than the average pressure vessel steel intended to be covered by the BPVC. In the past, ASME B31.12 has simply relied upon the the BPVC foundation to support our interest in certifying pipelines for hydrogen use. Given the difficulty (near impossibility) of manifesting compact tension specimens from ductile API pipeline materials which have the ability to create K_{IH} data acceptable per ASTM E1681, it is proposed here that the ASME B31.12 similarly amend the requirements to allow for both ASTM E1681 as well as ASTM E1820 testing.

Although option B exists, the testing involved is rigorous, costly, and therefore not often – perhaps never – implemented by end users. **There is now a push to provide a third option, Option C, within ASME B31.12 to allow for increased operating pressure.** This approach is based on both fatigue and fracture toughness data collected since the modification in 2019. The idea is that if we can characterize, for a large range of microstructures, the in-air ductility attributes (the Charpy transition curves and the fracture toughness, the carbon equivalent, the maximum hardness, and the centerline segregation) and correlate that information to performance in hydrogen, Option C would provide a suggested range of microstructures that are shown to be least susceptible to degradation by hydrogen.

ASME B31.12 does mention a few criteria specific to welds. Non-mandatory Appendix A recommends filler materials with similar chemical composition to base metal, as well as a recommendation that welds are either matched or over-matched. We believe the overmatching criteria may be a carry-over from natural gas recommendations in B31.8. However, it may be risky to over-match already higher strength steels for hydrogen.

Unless otherwise specified by engineering design, welding electrodes and filler metals used shall produce weld metal that complies with the following:

(a) Weld Metal Strength. The nominal tensile strength of the weld metal shall equal or exceed the minimum specified tensile strength of the base metals being joined.

(b) Differential Strength. If base metals of different tensile strengths are to be joined, the nominal tensile strength of the weld metal shall equal or exceed the minimum specified tensile strength of the weaker of the two.

(c) Weld Metal Chemical Analysis. The nominal chemical analysis of the weld metal shall be similar to the nominal chemical analysis of the major alloying elements of the base metal (e.g., 2 1⁄4% Cr, 1% Mo steels should be joined using 2 1⁄4% Cr, 1% Mo filler metals).

(d) Base Metal Chemical Analysis. If base metals of different chemical analysis are being joined, the nominal chemical analysis of the weld metal shall be similar to either base metal or an intermediate composition, except as specified below for austenitic steels joined to ferritic steels.

….

(h) Weldability Testing. Design engineering shall designate the tests to evaluate the susceptibility of the weld metal and heat affected zone to hydrogen cracking in accordance with ANSI/AWS B4.0.

(i) Diffusible Hydrogen Control. To control hydrogen induced cracking, the hydrogen level must be held to a certain maximum level. The applicable SFA-5.X filler metal specification electrodes, electrode-flux combinations, or electrodes and rods for gas-shielded arc welding capable of depositing weld metal with a maximum diffusible hydrogen content of 4 mL/100g (H4) are permitted. When purchasing electrodes and filler metal, the supplemental diffusible hydrogen designator shall be specified. An assessment of the diffusible hydrogen content is to be made according to one of the methods given in ANSI/AWS A4.3.

(j) Packaging. Electrodes shall be packaged in hermetically sealed containers.

Finally, ASME B31.12 non-mandatory Appendix G provides a guideline for producing steels with higher fracture toughness in hydrogen gas, based on work done at ORNL and SECAT with testing from Sandia, NIST, and PowerTech labs. These recommendations include limiting the carbon content and carbon equivalent, microalloying with niobium, limiting the centerline segregation during continuous casting, using thermo-mechanical control processing, and producing a steel with a grain size of ASTM 9 or finer. Now, these recommendations are for base metals, but of course the welding process complicates things. For example, while one may start with a fine-grained microstructure in the base metal, high heat inputs during the welding process can produce coarse grained heat affected zones which are well known to be among the worst microstructures for hydrogen susceptibility.

> *Microstructure plays an important role in achieving higher fracture toughness in the presence of gaseous hydrogen up to 20.7 MPa (3,000 psi). Alloy and steel processing design influences final steel microstructure formation. The desired steel microstructure is one of polygonal ferrite and acicular ferrite as uniformly distributed through the steel cross section. The following should be specified to obtain the desired steel microstructure:*
>
> *(a) Carbon content shall not exceed 0.07%.*
>
> *(b) The steel shall be niobium/columbium (Nb/Cb) microalloyed.*
>
> *(c) Carbon equivalent Pcm shall be as specified below:*
>
> *(1) API 5L X52 – X60, Pcm: 0.15% maximum*
>
> *(2) API 5L X65 – X80, Pcm: 0.17% maximum Pcm should be calculated by the following formula: Pcm = C + Si/30 + Mn/20 + Cu/20 + Ni/60 + Cr/20 + Mo/ 15 + V/10 + 5B*
>
> *(d) A slab macro etch test or other equivalent method shall be used to identify alloy centerline segregation during the continuous casting process. Use of sulfur prints is not an equivalent method. The slab macro etch test must be carried out on the first or second slab of each casting sequence and graded with an acceptance criterion of two maximum on the Mannesmann scale of 1 to 5 or equivalent.*
>
> *(e) Thermo Mechanical Control Processing (TMCP) shall be used in steel making.*
>
> *(f) Grain size shall be ASTM 9 or finer.*

Again, non-mandatory Appendix G was formed with base materials in mind, while the welding processes create a gradient of microstructures as one moves from the base, HAZ, and to weld. Although one may start with a base metal which adheres to non-mandatory Appendix G, different filler materials may impose different chemistries to the weld material. The welding process will create an HAZ which has often been observed to be more coarse-grained than the base metal. And the heat of the welding process may lead to chemical diffusion of species in the weld and the HAZ.

API 1104

API Standard 1104, *Welding Pipelines and Related Facilities*, covers requirements for gas and arc welding used in both the construction and the repair of pipes for the transmission of fuel gases and other products. Although API 1104 does not explicitly cover welding for pipelines for hydrogen transportation, ASME B31.12 and 49CFR Part 192 do refer to API 1104 for the qualification of welds for hydrogen service.

The majority of line pipe for hydrogen service will be delivered in TMCP condition according to API 1104 PSL2. API 1104 provides Annex G, which specifies additional provisions for PSL2 line pipe ordered for resistance to ductile fracture propagation in gas pipelines. The annex specifies minimum CVN energies the line pipe should have to provide ductile fracture propagation resistance.

API 1104 specifies a Charpy specimen v-notch location for HAZ impact testing, as shown in Figure 24. **This prescribed specimen placement necessarily has the crack path moving through multiple microstructures, including the weld metal, base metal, and all of the different HAZ zones (CG-HAZ, FG-HAZ, and IC-HAZ).**

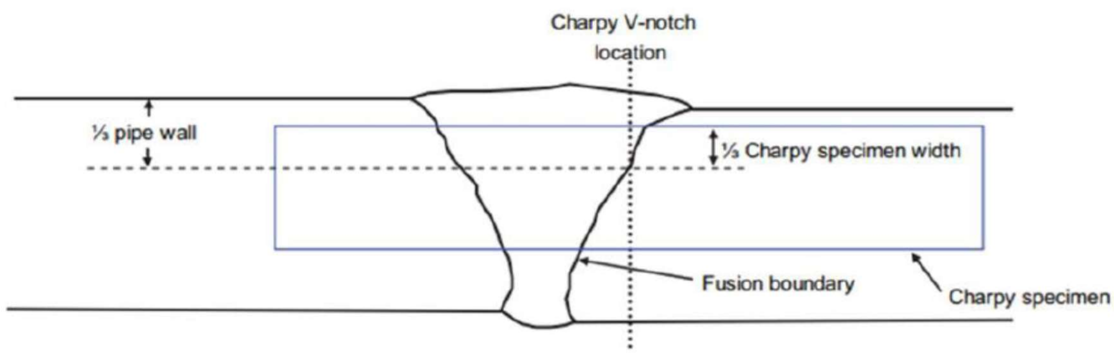

Figure 24: API 1104 Charpy specimen and v-notch location for HAZ impact testing.

As an example, the red line in Figure 25 illustrates the notch position for a Charpy specimen, which is aligned along the weld, the fusion line, the CG-HAZ, FG-HAZ, and finally, the base metal.

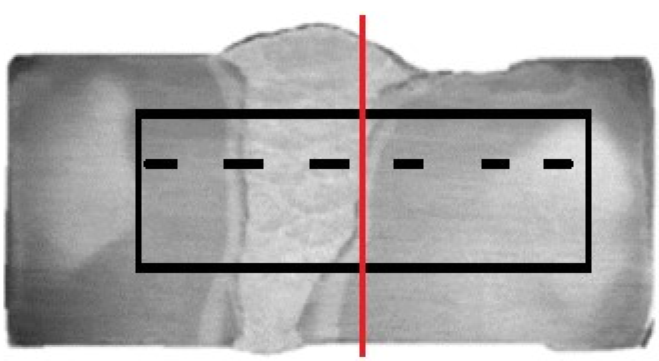

Figure 25: Charpy specimen placement for the weld in Example 1 from the Literature Review section of this report.

As mentioned in the literature review section, the measured Charpy energy is strongly dependent on notch position. As an assessment of material toughness in hydrogen, it is expected to be even more dependent on notch position, due to the drastic microstructure-dependence on hydrogen degradation of steels. Take for example the CG-HAZ in Case Example #2 from the literature review section. The narrow band of CG-HAZ lead to fracture instabilities in hydrogen fracture toughness tests, while in air the CG-HAZ retained significant resistance to fracture. **In that case, the API 1104 assessment of material performance through Charpy testing was not sufficient for hydrogen,** as the lowest toughness material would not be sufficiently isolated at the Charpy v-notch**.**

Regulatory Requirements Review

Code of Federal Regulations (CFR) 49 Part 192 – Transportation of Natural and Other Gas by Pipeline: Minimum Federal Safety Standards covers the minimum safety requirements for pipeline facilities and the transportation of gas. Currently hydrogen gas is not explicitly referenced in 49 CFR Part 192. Hydrogen sulfide (H_2S), however, is explicitly referenced. One reason for this may be that H_2S is poisonous in addition to promoting corrosion, however every reference to H_2S is in the context of controlling for internal corrosion, and hydrogen gas needs to be similarly considered in such a context.

§ 192.53 General.

Materials for pipe and components must be:

(a) Able to maintain the structural integrity of the pipeline under temperature and other environmental conditions that may be anticipated;

(b) Chemically compatible with any gas that they transport and with any other material in the pipeline with which they are in contact; and

(c) Qualified in accordance with the applicable requirements of this subpart.

§ 192.55 Steel pipe.

(a) New steel pipe is qualified for use under this part if:

(1) It was manufactured in accordance with a listed specification;

(2) It meets the requirements of –

(i) Section II of appendix B to this part; or

(ii) If it was manufactured before November 12, 1970, either section II or III of appendix B to this part; or

(3) It is used in accordance with paragraph (c) or (d) of this section.

(b) Used steel pipe is qualified for use under this part if:

(1) It was manufactured in accordance with a listed specification and it meets the requirements of paragraph II-C of appendix B to this part;

(2) It meets the requirements of:

(i) Section II of appendix B to this part; or

(ii) If it was manufactured before November 12, 1970, either section II or III of appendix B to this part;

(3) It has been used in an existing line of the same or higher pressure and meets the requirements of paragraph II-C of appendix B to this part; or

(4) It is used in accordance with paragraph (c) of this section.

(c) New or used steel pipe may be used at a pressure resulting in a hoop stress of less than 6,000 p.s.i. (41 MPa) where no close coiling or close bending is to be

done, if visual examination indicates that the pipe is in good condition and that it is free of split seams and other defects that would cause leakage. If it is to be welded, steel pipe that has not been manufactured to a listed specification must also pass the weldability tests prescribed in paragraph II-B of appendix B to this part.

(d) Steel pipe that has not been previously used may be used as replacement pipe in a segment of pipeline if it has been manufactured prior to November 12, 1970, in accordance with the same specification as the pipe used in constructing that segment of pipeline.

(e) New steel pipe that has been cold expanded must comply with the mandatory provisions of API Spec 5L (incorporated by reference, see § 192.7).

The majority of steel line pipe will be manufactured according to API 5L specifications. If not, section II of Appendix B requires test welds or alternatively chemical compatibility with welding processes:

B. ***Weldability.*** *A girth weld must be made in the pipe by a welder who is qualified under subpart E of this part. The weld must be made under the most severe conditions under which welding will be allowed in the field and by means of the same procedure that will be used in the field. On pipe more than 4 inches (102 millimeters) in diameter, at least one test weld must be made for each 100 lengths of pipe. On pipe 4 inches (102 millimeters) or less in diameter, at least one test weld must be made for each 400 lengths of pipe. The weld must be tested in accordance with API Standard 1104 (incorporated by reference, see § 192.7). If the requirements of API Standard 1104 cannot be met, weldability may be established by making chemical tests for carbon and manganese, and proceeding in accordance with section IX of the ASME Boiler and Pressure Vessel Code (ibr, see 192.7). The same number of chemical tests must be made as are required for testing a girth weld.*

Subpart C of 49 CFR Part 192 prescribes a design pressure based on the yield strength, wall thickness, outside diameter, and three design factors:

§ 192.105 Design formula for steel pipe.

The design pressure for steel pipe is determined in accordance with the following formula:

$$P = (2\ S\ t/D) \times F \times E \times T$$

P = Design pressure in pounds per square inch (kPa) gauge.
S = Yield strength in pounds per square inch (kPa) determined in accordance with § 192.107.
D = Nominal outside diameter of the pipe in inches (millimeters).
t = Nominal wall thickness of the pipe in inches (millimeters). If this is unknown, it is determined in accordance

with § 192.109. Additional wall thickness required for concurrent external loads in accordance with § 192.103
may not be included in computing design pressure.
F = Design factor determined in accordance with § 192.111.
E = Longitudinal joint factor determined in accordance with § 192.113.
T = Temperature derating factor determined in accordance with § 192.115.

Design factor *F* derates the maximum allowed pressure based on the location of pipe, while design factor *E* places design penalties on some pipeline weld classes, in particular on furnace butt-welded pipe manufactured according to ASTM A 53/A53M or API 5L. Pipes over 4 inches in diameter has a longitudinal joint factor which is greater than pipe less than 4 inches (*E = 0.8* compared to *E* = 0.6). Design factor *T* derates the design pressure according to the transport gas temperature. **Of note, the derating factor T above 400 F (204 C) ranges from 0.900 – 0.867. Because 49 CFR Part 192 does not explicitly address hydrogen, High Temperature Hydrogen Attack (HTHA), a mechanism of hydrogen-assisted damage which severely degrades steels at temperatures above 400 F, is not fully addressed with the derating factor T, as HTHA begins to severely degrade steels at temperatures above 400 F. Although HTHA is outside of the scope of this project, this highlights the potential issues that may arise by not explicitly addressing hydrogen in 49 CFR Part 192.**

The design pressure calculation in 49 CFR Part 192 is identical to the design pressure calculation in ASME B31.12 PL-3.7.1, except that the latter adds an additional material performance factor, H_f (see Figure 22). Note that if Option B under ASME B31.12 PL-3.7.1 is used, H_f is taken to be 1.0. However, 49 CFR Part 192 only requires an incorporation of H_f into the design pressure if the pipeline is intended to exceed the maximum allowable operating pressure (MAOP), under 49 CFR Part 192.112:

§ 192.112 Additional design requirements for steel pipe using alternative maximum allowable operating pressure.
For a new or existing pipeline segment to be eligible for operation at the alternative maximum allowable operating pressure (MAOP) calculated under § 192.620, a segment must meet the following additional design requirements. Records for alternative MAOP must be maintained, for the useful life of the pipeline, demonstrating compliance with these requirements:
The pipeline segment must meet these additional requirements:
(a) General
(1) The plate, skelp, or coil used for the pipe must be micro-alloyed, fine grain, fully killed, continuously cast steel with calcium treatment.
(2) The carbon equivalents of the steel used for pipe must not exceed 0.25 percent by weight, as calculated by the Ito-Bessyo formula (Pcm formula) or 0.43 percent by weight, as calculated by the International Institute of Welding (IIW) formula.
(3) The ratio of the specified outside diameter of the pipe to the specified wall thickness must be less than 100. The wall thickness or other mitigative measures must prevent denting and ovality anomalies during construction, strength testing and anticipated operational stresses.

(4) The pipe must be manufactured using API Spec 5L, product specification level 2 (incorporated by reference, see § 192.7) for maximum operating pressures and minimum and maximum operating temperatures and other requirements under this section.

(b) Fracture control

(1) The toughness properties for pipe must address the potential for initiation, propagation and arrest of fractures in accordance with:

(i) API Spec 5L (incorporated by reference, see § 192.7); or

(ii) American Society of Mechanical Engineers (ASME) B31.8 (incorporated by reference, see § 192.7); and

(iii) Any correction factors needed to address pipe grades, pressures, temperatures, or gas compositions not expressly addressed in API Spec 5L, product specification level 2 or ASME B31.8 (incorporated by reference, see § 192.7).

Therefore, ASME B31.12 is only referenced indirectly through 192.112 b-1-iii, and only pipelines using an alternative MAOP will be required to utilize the material design factor H_f, though ASME B31.12 utilizes H_f for all design pressures under Option A of Pl-3.7.1.

(2) Fracture control must:

(i) Ensure resistance to fracture initiation while addressing the full range of operating temperatures, pressures, gas compositions, pipe grade and operating stress levels, including maximum pressures and minimum temperatures for shut-in conditions, that the pipeline is expected to experience. If these parameters change during operation of the pipeline such that they are outside the bounds of what was considered in the design evaluation, the evaluation must be reviewed and updated to assure continued resistance to fracture initiation over the operating life of the pipeline;

(ii) Address adjustments to toughness of pipe for each grade used and the decompression behavior of the gas at operating parameters;

(iii) Ensure at least 99 percent probability of fracture arrest within eight pipe lengths with a probability of not less than 90 percent within five pipe lengths; and

(iv) Include fracture toughness testing that is equivalent to that described in supplementary requirements SR5A, SR5B, and SR6 of API Specification 5L (incorporated by reference, see § 192.7) and ensures ductile fracture and arrest with the following exceptions:

(A) The results of the Charpy impact test prescribed in SR5A must indicate at least 80 percent minimum shear area for any single test on each heat of steel; and

(B) The results of the drop weight test prescribed in SR6 must indicate 80 percent average shear area with a minimum single test result of 60 percent shear area for any steel test samples. The test results must ensure a ductile fracture and arrest.

(3) If it is not physically possible to achieve the pipeline toughness properties of paragraphs (b)(1) and (2) of this section, additional design features, such as

mechanical or composite crack arrestors and/or heavier walled pipe of proper design and spacing, must be used to ensure fracture arrest as described in paragraph (b)(2)(iii) of this section.

While 49 CFR Part 192 limits the maximum hardness at the seam weld to 280 Vickers, ASME B31.12 limits the hardness to 235 Vickers:

(d) Seam quality control

(1) There must be a quality assurance program for pipe seam welds to assure tensile strength provided in API Spec 5L (incorporated by reference, see § 192.7) for appropriate grades.

(2) There must be a hardness test, using Vickers (Hv10) hardness test method or equivalent test method, to assure a maximum hardness of 280 Vickers of the following:

(i) A cross section of the weld seam of one pipe from each heat plus one pipe from each welding line per day; and

(ii) For each sample cross section, a minimum of 13 readings (three for each heat affected zone, three in the weld metal, and two in each section of pipe base metal).

(3) All of the seams must be ultrasonically tested after cold expansion and mill hydrostatic testing.

Material Identification and Phase II Test Matrix

Overall approach

In light of the complicated effect of microstructure outlined in the literature review, the approach of a proposed "Option C" outlined in the Codes and Standards review, and the lack of explicit mention to hydrogen in 49 CFR Part 192 outlined in the Regulatory review, we propose a three-pronged approach for a microstructure-based understanding of hydrogen effects on pipeline welds, as depicted in Figure 26. The first approach will be to study real, modern pipeline welds solicited from industry partners with the aim of exploring as wide of a spectrum of microstructures as possible. Although this data will provide critical information on the effect of hydrogen on specific microstructures, it is important to link these microstructures to specific welding parameters. Therefore, the second and third approaches will be systematic studies of two key welding parameters: the weld filler material, including both standard filler materials as well as exploratory filler materials, and the thermal cycling parameters of maximum temperature and cooling rate. By providing data on the effect of hydrogen on different microstructures, as well as the processes which generate those microstructures, we will provide guidance to the pipeline welding community for generating hydrogen-resistant pipeline welds. A thorough study of the effect of thermal cycling parameters will also allow us to determine hydrogen effects on repair welds.

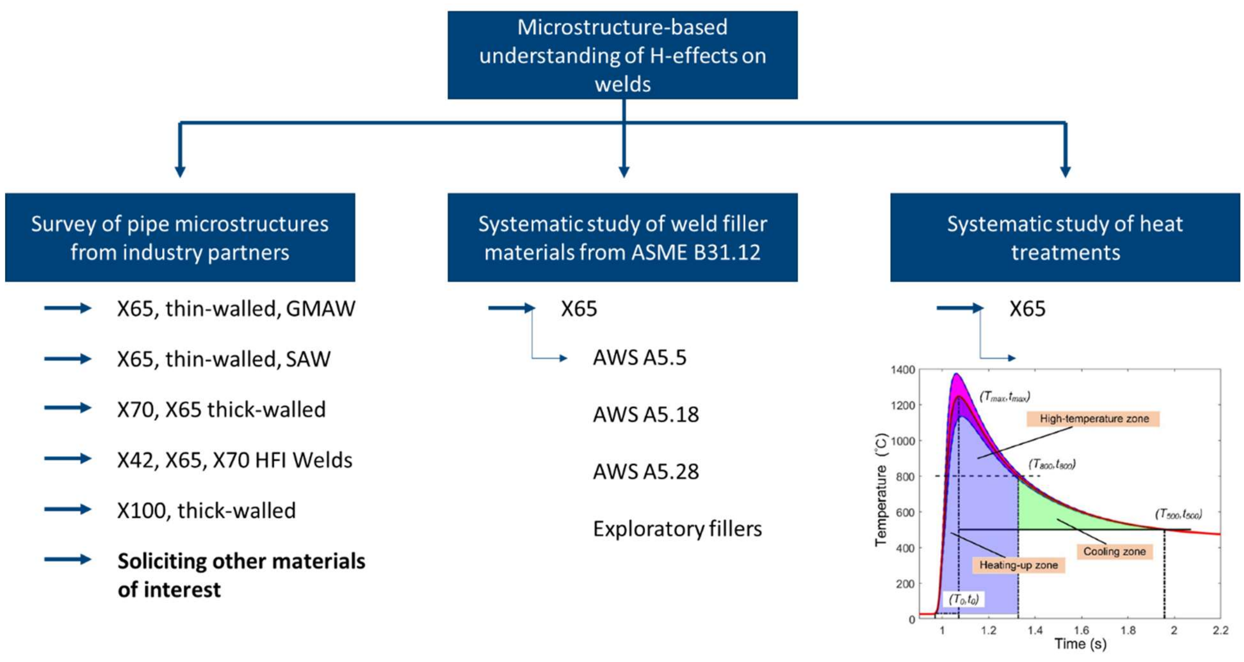

Figure 26: Overall approach to Phase II of this work.

To assess the performance of these microstructures in hydrogen gas, we will perform Charpy impact tests as directed in API 1104, ASTM E1820 fracture toughness tests as outlined in ASME B31.12, PL-3.7.1 Option B, and hardness maps to assess the appropriateness of the limit in ASME B31.12. ASTM E1820 fracture toughness tests in hydrogen are by far the most time-intensive tests within this test matrix. To allow for a sufficient number of tests to update the codes and standards, the testing efficiency at NIST needed to be improved. To increase the efficiency, we are developing an SEN(B) fixture for the E1820 tests. The SEN(B) geometry will decrease the amount of material necessary for specimens compared to C(T) geometry tests. Additionally, SEN(B) tests can be performed in the smallest of NIST's two chambers. Running tests in the smaller of the two chambers decreases the time required for the purging procedure from approximately one day, to approximately 1-2 hours, and will allow multiple tests to be performed per day compared to just a few per week. The fixture design was constrained by the limited space inside the smaller chamber, and a preference for the SEN(B) tests to be performed in tension rather than compression. The design for the fixture is shown in Figure 27.

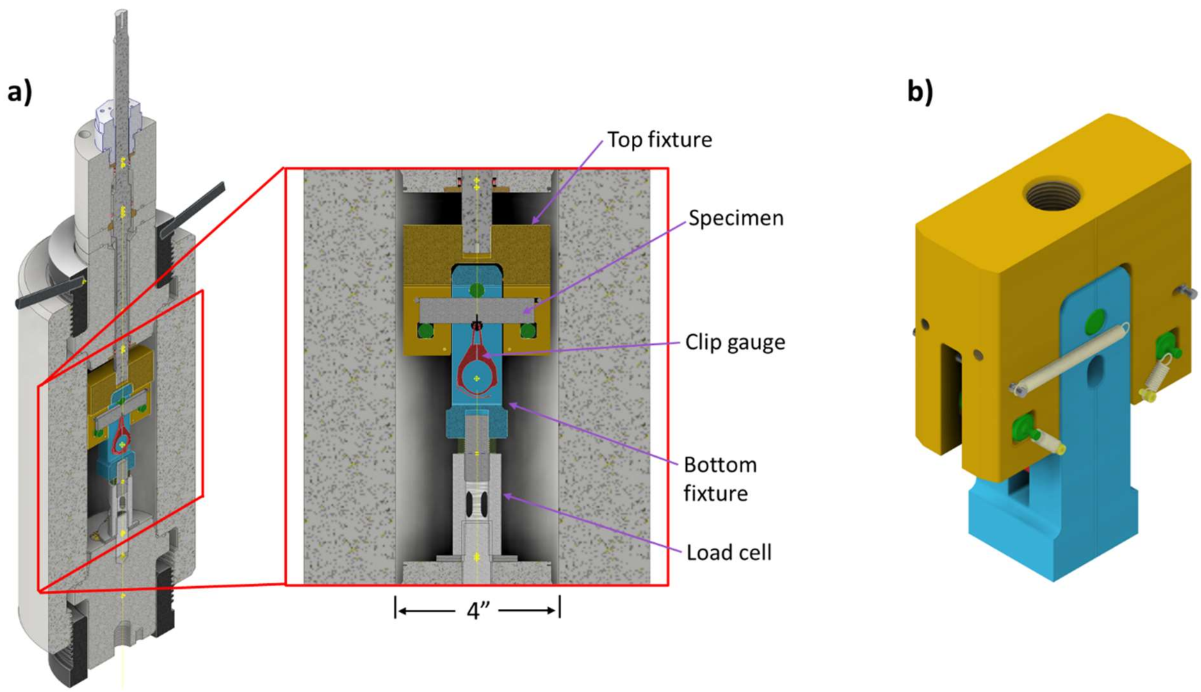

Figure 27: SEN(B) fixture, specially designed for ASTM E1820 tests in hydrogen gas. Testing SEN(B) will increase the efficiency of testing at NIST-Boulder, increasing the number of tests during Phase II by a factor of 4.

Industry Survey

As of the submission of this Phase I report, we have solicited ten pipes from various industrial contacts, mostly through contacts within the API 1104 committee. The materials collected include both seam and girth welds, encompassing 6 different wall thicknesses, 5 pipe diameters, 3 material grades, a range of Nb content from 0 % to 0.70%, and low to high Charpy energies and Charpy standard deviations. The spider-plot in Figure 28 depicts the range of materials solicited so far.

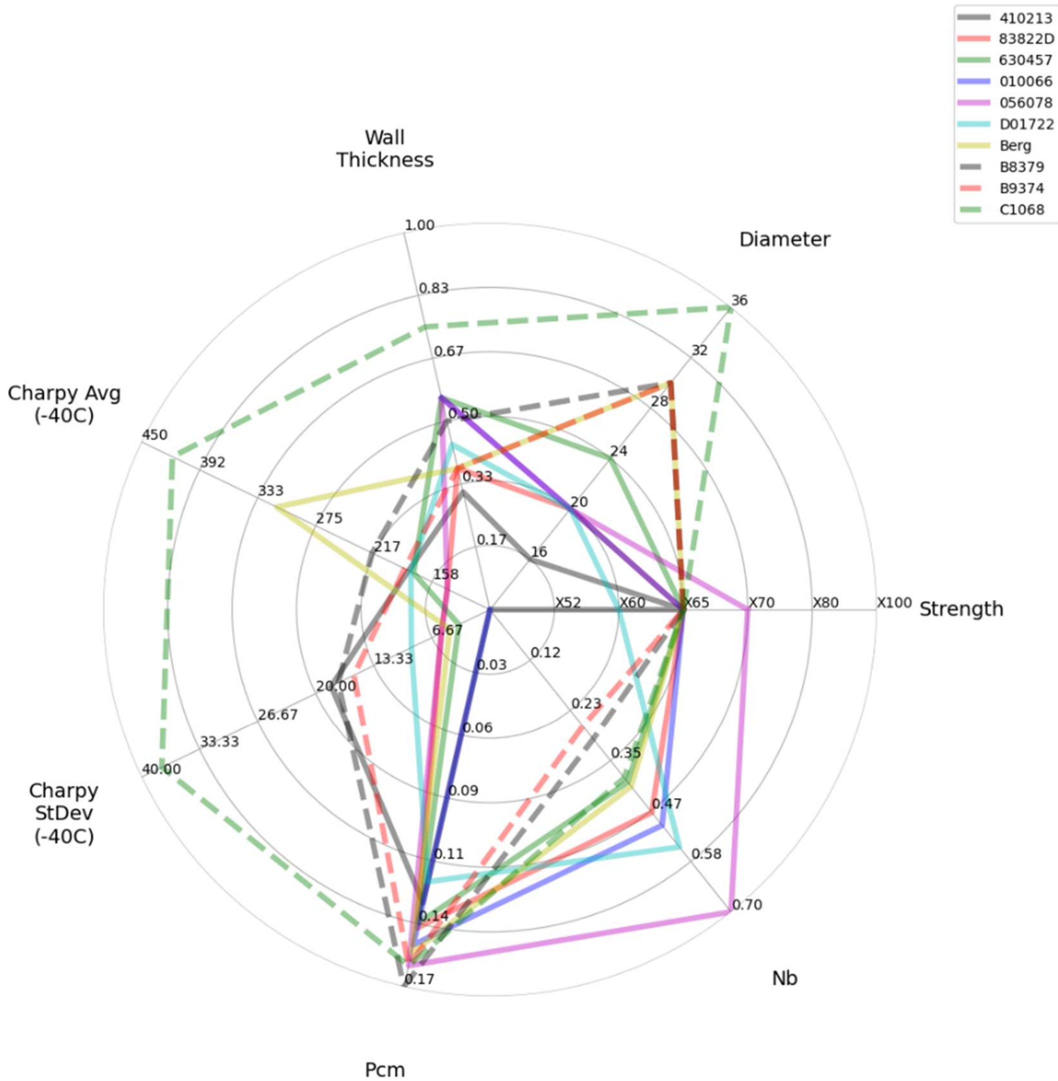

Figure 28: Spider-plot of different materials solicited from industry partners for study in Phase II.

To demonstrate the range of HAZ microstructures available in the industry survey portion of this work, Figure 29 show optical micrographs of each weld near the fusion line. The Berg pipe weld and B8 pipe weld show a large CG-HAZ near the weld fusion line, extending across hundreds of micrometers. The B9 pipe weld and C1 pipe weld show relatively limited CG-HAZs.

The CG-HAZs have some grains which appear to be composed of lathe-like structures, suggesting that martensite has been formed.

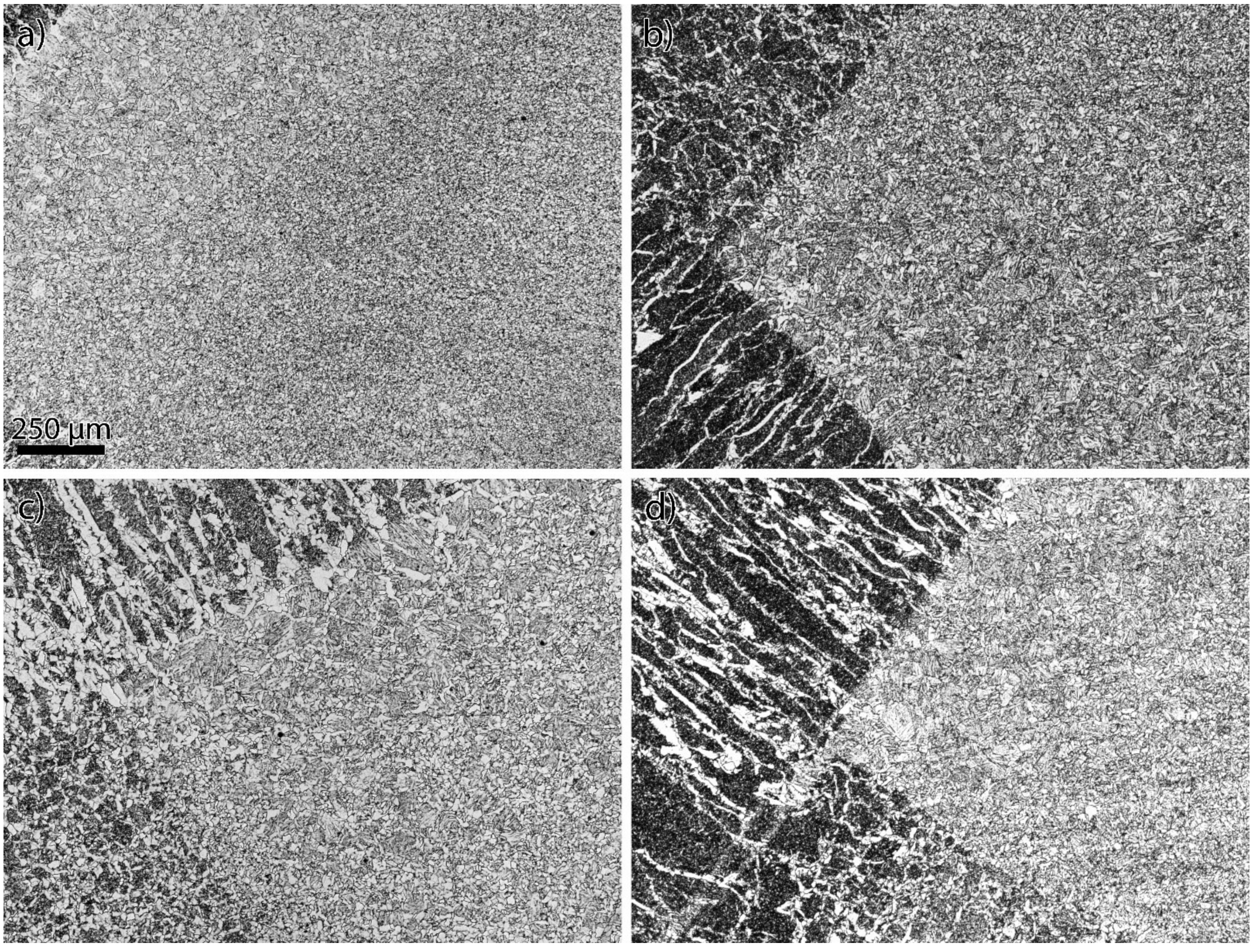

Figure 29: Optical images of weld and HAZ microstructures to be studied in Phase II of this work. A) Berg pipe, B) B8 pipe, C) B9 pipe, and D) C1 pipe.

Welds without filler material are also included in our study, a portion of which are shown in Figure 30~~Figure 30~~, which were created through High-Frequency Induction (HFI). These HFI welds show remarkable little variation in microstructure across the weld, HAZ, and base material. Near the weld fusion line, the grain structures appear to develop some preferred orientation, with the orientation of the grains aligning with the weld fusion line. While the lack of a large-grained CG-HAZ is promising for the use of hydrogen with these welds, this preferred orientation of the grains provides a potential pathway for large cracks to develop. Therefore, it remains to be seen how these HFI welds will perform in hydrogen compared to welds created with filler materials.

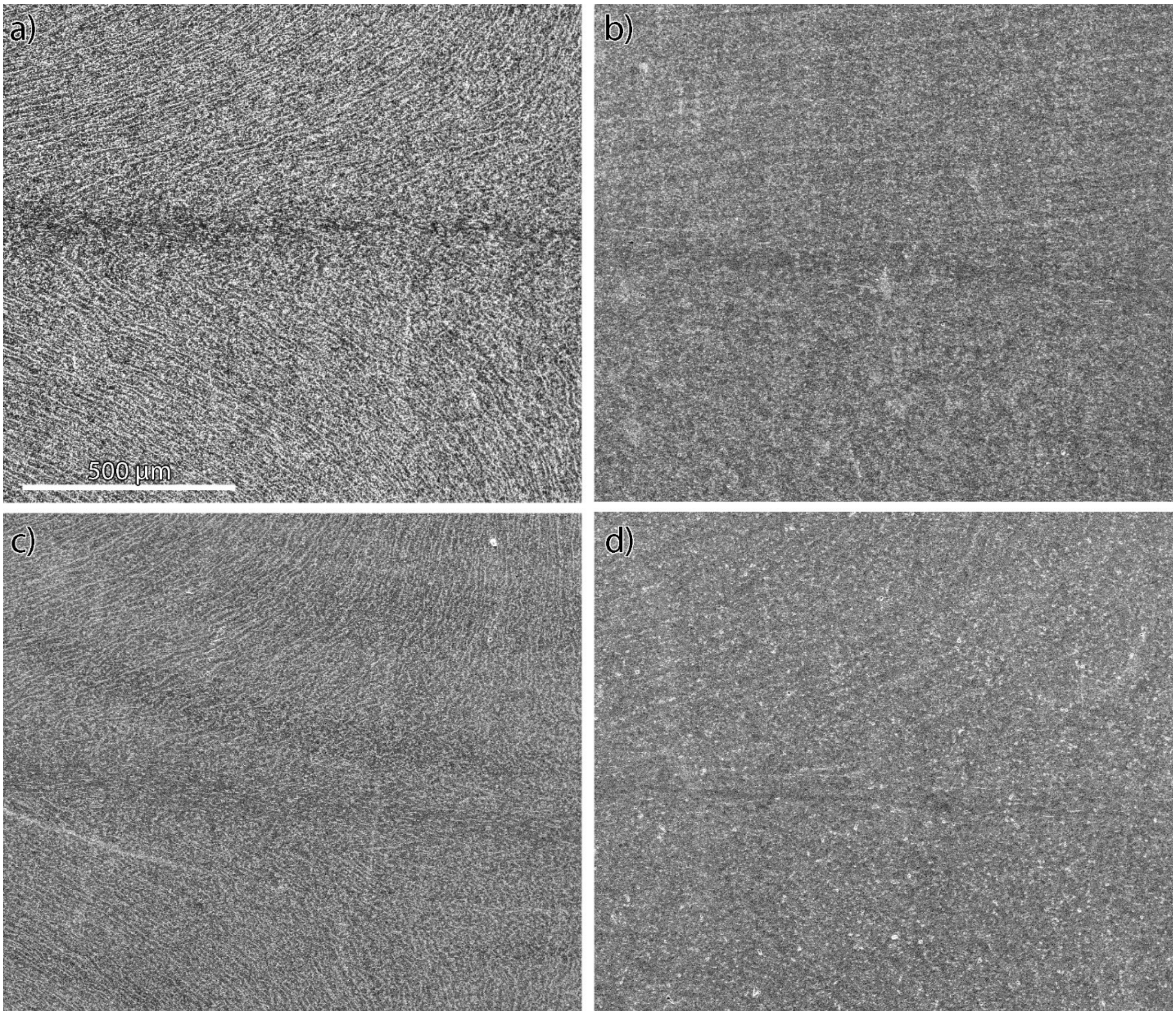

Figure 30: Fusion lines from various HFI welds to be studied during Phase II of this work.

Weld Filler Material Study

As noted in the Literature Review section, the microstructure of the weld depends in part on the chemistry of the filler material. ASME B31.12 refers to API 1104 for acceptable weld filler materials for pipelines for hydrogen service. For GTAW or GMAW welds, for example, typical weld filler materials conform to American Welding Society (AWS) standard A5.18. With AWS A5.18, concentration ranges of many alloying elements are listed, however the largest differences are in Mn and Si concentration. Figure 31~~Figure 37~~ and Figure 32~~Figure 38~~ show the ranges of Mn and Si concentration allowed under AWS A5.18. We will explore the impact of choice of filler material in our testing matrix by testing welds created using filler material ER70S-X where X= [2-7].

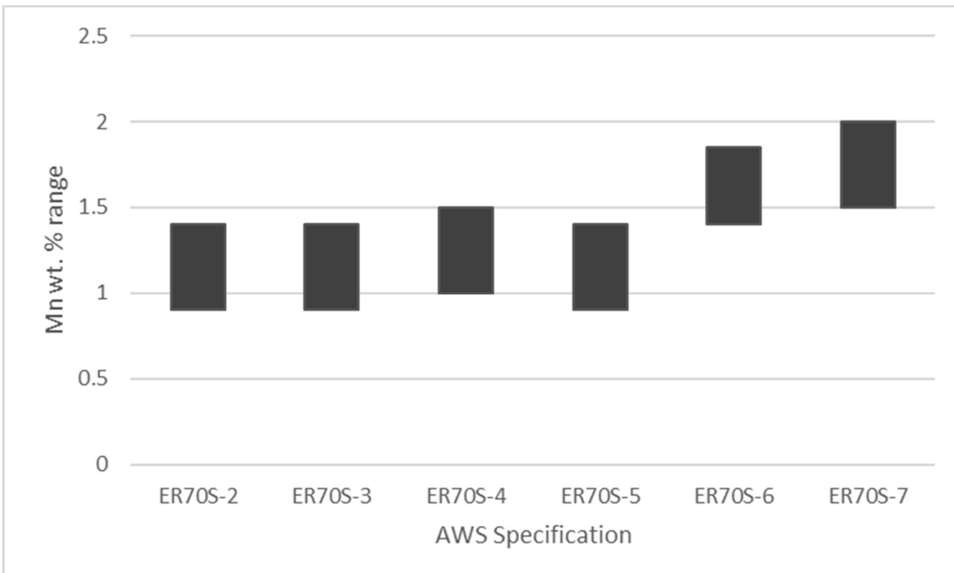

Figure 31: Ranges of Mn concentrations in standard welding filler materials allowed by ASME B31.12.

Figure 32: Ranges of Si concentrations in standard welding filler materials allowed by ASME B31.12.

Additionally, AWS lists a filler material specification ER70S-G which does not have standard chemistry ranges but allows for other, perhaps proprietary, weld filler material alloying element concentrations. One particular alloying element of interest is Nb. Non-mandatory Appendix G of ASME B31.12 suggests Nb as an alloying element for base material. Additionally, recent work has shown additions of Nb can reduce the grain size of the CGHAZ [61], which may (or may not) be beneficial for retaining toughness when exposed to hydrogen gas. In addition to testing welds made with AWS standard filler materials, our testing matrix will include filler materials with Nb additions to study the effect.

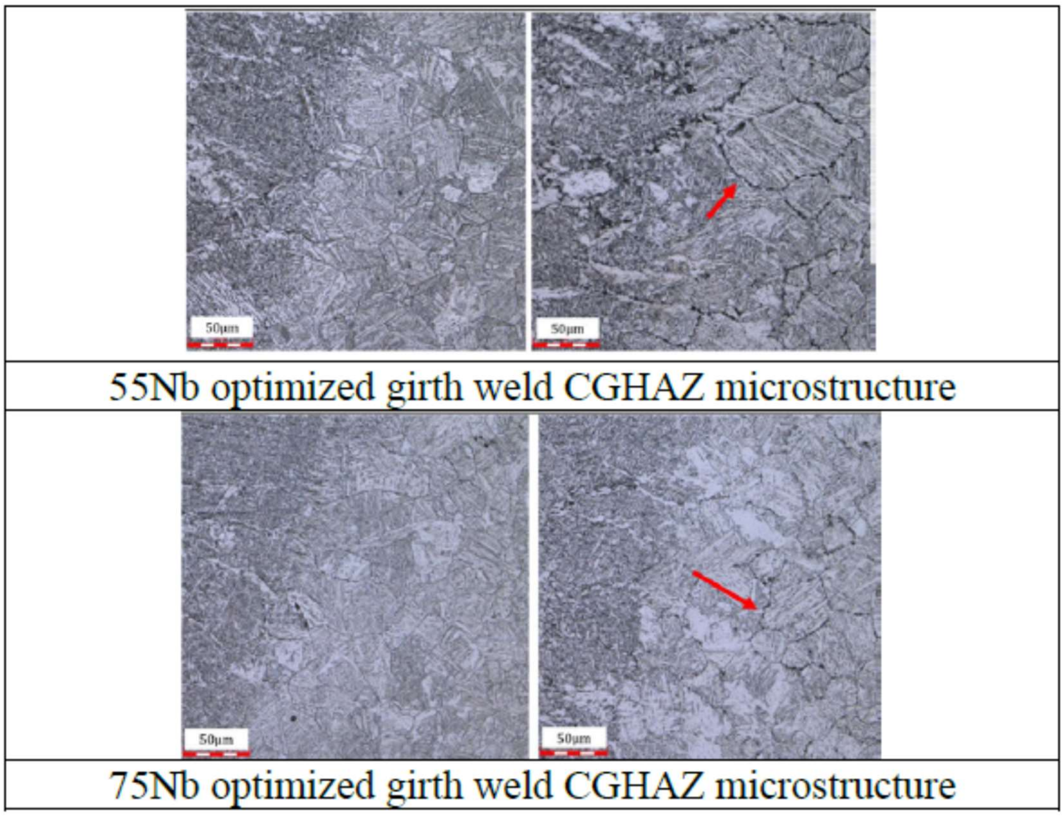

Figure 33: Girth weld microstructures for two steels with different Nb concentrations.

Weld Thermal Cycling Study

The interaction of hydrogen with steel is highly dependent on both the chemistry and the microstructure of the metal. Welding thermal parameters (e.g. maximum temperature and cooling rate) play a critical role in determining the microstructure in welds and heat affected zones of the base metal. A systematic study of the effect of welding thermal parameters on the microstructure of steel, followed by a measurement of the hydrogen effects on those microstructures, provides a pathway for providing industry recommended welding parameters for pipelines intended for hydrogen service.

The objective of this work is to simulate a wide spectrum of steel microstructures which are linked to thermal cycling parameters, and to mechanically test these simulated specimens in high pressure hydrogen gas. In this way, we will provide pipeline manufacturers the key ingredients (weld parameters) for producing pipeline welds which are least susceptible to degradation from hydrogen.

T (Celsius)	Cooling Rate
1300	Air Cooled
1225	Air Cooled
1150	Air Cooled
1075	Air Cooled
1000	Air Cooled
900	Air cooled
800	Air Cooled
T1 (tbd)	Cooling Rate tbd 1
T1 (tbd)	Cooling Rate tbd 1
T1 (tbd)	Cooling Rate tbd 1
T2 (tbd)	Cooling Rate tbd 2
T2 (tbd)	Cooling Rate tbd 2
T2 (tbd)	Cooling Rate tbd 2
T3 (tbd)	Cooling Rate tbd 3
T3 (tbd)	Cooling Rate tbd 3
T3 (tbd)	Cooling Rate tbd 3

Figure 34: Test matrix for thermal cycling parameter study for Phase II of this work.

A total of 144 samples representing 16 different thermal cycling parameters is planned to be generated using a Gleeble thermomechanical simulator at Mines. Sample geometry design will be optimized using finite element simulation (FEM). The test matrix will be designed based on thermodynamic calculations and metallurgical characterizations on the received pipeline steel weldments. The test matrix is planned to include 7 maximum temperatures which will have variable cooling rates through ambient air cooling. From these, 3 maximum temperatures will be selected for a study of cooling rates with 3 controlled cooling rates each. The microstructures of each sample condition will be characterized through optical microscopy and scanning electron microscopy (SEM). For each condition, three samples will be used to measure the upper-shelf Charpy impact energy, three samples will be used to measure the fracture toughness in air, and three samples will be used to measure the fracture toughness in 3000 psi (21 MPa) hydrogen gas.

Gleeble thermomechanical simulator has been used to simulate HAZ microstructures for previous studies, including a small number for tests in hydrogen. This present work will expand on this work by performing a large, systematic study connecting weld thermal parameters with hydrogen performance.

Industry and Subject Matter Expert Committee

Person	Organization	Email
Robert Smith	DOT/PHMSA	Robert.W.Smith@dot.gov
Brady Dague	DOT/PHMSA	brady.dague@dot.gov
Mark Richards	DOE	mark.richards@ee.doe.gov
Chris San Marchi	Sandia	cwsanma@sandia.gov
Vincent Holohan	DOT/PHMSA	Vincent.Holohan@dot.gov
Aaron Litschewski	CBMM	aaron.litschewski@cbmm.com
Nathan Regdos	National Fuel	regdosn@natfuel.com
Ken Lee	DNV	Ken.lee@dnv.com
Rick Noecker	ExxonMobil / API 1104	rick.noecker@exxonmobil.com
Simon Gant	HSE (UK Gov Research)	Simon.coldrick@hse.gov.uk
Otto Jan Huising	Gasunie/ EPRG Task Group on H2	O.J.C.Huising@gasunie.nl
Martin Connelly	Liberty Pipes	martin.connelly@libertysteelgroup.com
Dan Peters	ASME Hydrogen for a Green Economy Steering Committee / Struct Int	dpeters@structint.com
Ryan Crane	ASME Hydrogen for a Green Economy Steering Committee	craneR@asme.org
Paul Spielbauer	Lake Superior Consulting / API 1104 H2 Fuel Gas Pipeline Co-chair	pspielbauer@LSConsulting.com
Mike Childers	Southwest Gas / API 1104	mike.childers@swgas.com
Doug Stalheim	B31.12	dgstalheim@comcast.net
Zhenzhen Yu	Colorado School of Mines	zyu@mines.edu

Jonah Klemm-Toole	Colorado School of Mines	jklemmto@mines.edu

Related Work

NIST is aware of related work through API 1104 and EWI “Assessing Hardness Limits for Pipe Steels Under Hydrogen Gas Exposure”. The scope of this work is separated into two main tasks. The first is to evaluate crack initiation susceptibility and correlate this with hardness. This portion of the project will utilize four-point bend tests of crack initiation at a test pressure of 3000 psi on specimens made using Gleeble simulator. In the second task, EWI and Sandia National Labs will perform tests of K_{IH} on a select number of specimens from the first task.

Phase II of this work will attempt to provide a broad assessment of the effect of hydrogen on a wide spectrum of weld and HAZ microstructures. In the process, we will collect both hardness maps as well as fracture toughness data in hydrogen gas. Given the overlap and as the data collected in Phase II will be critical to the related work from API 1104 and EWI, NIST will share the data collected in Phase II with the PIs of the related work, as well as through the Industry and Subject Matter Expert Committee.

References

1. *API 1104: Welding of Pipelines and Related Facilities*. 2021: American Petrolium Institute.
2. *API Specification 5L*. Line Pipe. 2018: American Petroleum Institute.
3. *ASME B31.8*. Gas Transmission and Distribution Piping Sytems. 2018: ASME International.
4. *ASME B31.12*. Hydrogen Piping and Pipelines. 2019: ASME International.
5. *Code of Federal Regulations*

Title 49, Transportation, Part 192, Transportation of Natural and Other Gas by Pipeline: Minimum Federal Safety Standards. 2023, U.S. Department of Transportation: Washington, DC.

6. Gillette, J. and R. Kolpa, *Overview of interstate hydrogen pipeline systems*. 2008, Argonne National Lab.(ANL), Argonne, IL (United States).
7. Noecker, R., *Taxonomy of Modern Line Pipe and Girth Welds*. 2023.
8. Johnson, W.H., *On some remarkable changes produced in iron and steel by the action of hydrogen and acids.* Nature, 1875. **11**(281): p. 393.
9. Kirchheim, R. and A. Pundt, *Hydrogen in metals Physical Metallurgy*. 2014, Amsterdam: Elsevier.
10. Koyama, M., et al., *Recent progress in microstructural hydrogen mapping in steels: quantification, kinetic analysis, and multi-scale characterisation.* Materials Science and Technology, 2017. **33**(13): p. 1481-1496.
11. Moro, I., et al., *Hydrogen embrittlement susceptibility of a high strength steel X80.* Materials Science and Engineering: A, 2010. **527**(27-28): p. 7252-7260.
12. Jewett, R.P., et al., *Hydrogen environment embrittlement of metals*. 1973.
13. Cialone, H.J. and J.H. Holbrook, *Sensitivity of steels to degradation in gaseous hydrogen*. 1988: ASTM International Philadelphia, PA, USA.
14. Cialone, H. and J. Holbrook, *Effects of gaseous hydrogen on fatigue crack growth in pipeline steel.* Metallurgical Transactions A, 1985. **16**: p. 115-122.
15. Drexler, E.S., et al., *Fatigue crack growth rates of API X70 pipeline steel in a pressurized hydrogen gas environment.* Fatigue & Fracture of Engineering Materials & Structures, 2014. **37**(5): p. 517-525.
16. Slifka, A.J., et al., *Fatigue measurement of pipeline steels for the application of transporting gaseous hydrogen.* Journal of Pressure Vessel Technology, 2018. **140**(1).
17. Amaro, R.L., et al., *Development of a model for hydrogen-assisted fatigue crack growth of pipeline steel.* Journal of Pressure Vessel Technology, 2018. **140**(2).
18. Barthélémy, H., *Effects of pressure and purity on the hydrogen embrittlement of steels.* International Journal of Hydrogen Energy, 2011. **36**(3): p. 2750-2758.
19. Stalheim, D., et al. *Continued microstructure and mechanical property performance evaluation of commercial grade API pipeline steels in high pressure gaseous hydrogen*. in *International Pipeline Conference*. 2012. American Society of Mechanical Engineers.
20. Nibur, K., et al. *Measurement of sustained-load cracking thresholds for steels in hydrogen delivery and storage*. in *ASME Pressure Vessels and Piping Conference*. 2008.
21. Martin, M.L., et al., *Evaluating a natural gas pipeline steel for blended hydrogen service.* Journal of Natural Gas Science and Engineering, 2022. **101**: p. 104529.

22. Lam, P., et al., *Literature survey of gaseous hydrogen effects on the mechanical properties of carbon and low alloy steels.* Journal of pressure vessel technology, 2009. **131**(4).
23. Stalheim, D., et al. *Microstructure and mechanical property performance of commercial grade API pipeline steels in high pressure gaseous hydrogen*. in *International Pipeline Conference*. 2010.
24. San Marchi, C., et al. *Fracture and fatigue of commercial grade API pipeline steels in gaseous hydrogen*. in *Pressure Vessels and Piping Conference*. 2010.
25. San Marchi, C., B.P. Somerday, and S.L. Robinson, *Permeability, solubility and diffusivity of hydrogen isotopes in stainless steels at high gas pressures.* International Journal of Hydrogen Energy, 2007. **32**(1): p. 100-116.
26. Martin, M.L., et al., *Hydrogen embrittlement in ferritic steels.* Applied physics reviews, 2020. **7**(4): p. 041301.
27. Johnson, H., J. Morlet, and A. Troiano, *Hydrogen, crack initiation, and delayed failure in steel.* Trans. Met. Soc. AIME, 1958. **212**.
28. Oriani, R., *Whitney award lecture—1987: hydrogen—the versatile embrittler.* Corrosion, 1987. **43**(7): p. 390-397.
29. Oriani, R. and P. Josephic, *Equilibrium aspects of hydrogen-induced cracking of steels.* Acta metallurgica, 1974. **22**(9): p. 1065-1074.
30. Gemma, R., et al., *APT analyses of deuterium-loaded Fe/V multi-layered films.* Ultramicroscopy, 2009. **109**(5): p. 631-636.
31. Ronevich, J.A., B.P. Somerday, and C.W. San Marchi, *Effects of microstructure banding on hydrogen assisted fatigue crack growth in X65 pipeline steels.* International Journal of Fatigue, 2016. **82**: p. 497-504.
32. Wang, J.J.-A., et al., *The development of in situ fracture toughness evaluation techniques in hydrogen environment.* International Journal of hydrogen energy, 2015. **40**(4): p. 2013-2024.
33. Drexler, E.S., et al., *Fatigue testing of pipeline welds and heat-affected zones in pressurized hydrogen gas.* Journal of Research of the National Institute of Standards and Technology, 2019. **124**: p. 1.
34. Ronevich, J.A., B.P. Somerday, and Z. Feng, *Hydrogen accelerated fatigue crack growth of friction stir welded X52 steel pipe.* International Journal of Hydrogen Energy, 2017. **42**(7): p. 4259-4268.
35. Olden, V., A. Alvaro, and O.M. Akselsen, *Hydrogen diffusion and hydrogen influenced critical stress intensity in an API X70 pipeline steel welded joint–Experiments and FE simulations.* International journal of hydrogen energy, 2012. **37**(15): p. 11474-11486.
36. Nagumo, M., M. Nakamura, and K. Takai, *Hydrogen thermal desorption relevant to delayed-fracture susceptibility of high-strength steels.* Metallurgical and Materials Transactions A, 2001. **32**: p. 339-347.
37. Martin, M.L., et al., *Enumeration of the hydrogen-enhanced localized plasticity mechanism for hydrogen embrittlement in structural materials.* Acta Materialia, 2019. **165**: p. 734-750.
38. Robertson, I.M., et al., *Hydrogen embrittlement understood.* Metallurgical and Materials Transactions A, 2015. **46**: p. 2323-2341.
39. Tabata, T. and H. Birnbaum, *Direct observations of hydrogen enhanced crack propagation in iron.* Scr. Metall.;(United States), 1984. **18**(3).

40. Ferreira, P., I.M. Robertson, and H. Birnbaum. *Influence of hydrogen on the stacking-fault energy of an austenitic stainless steel*. in *Materials Science Forum*. 1996.
41. Birnbaum, H.K. and P. Sofronis, *Hydrogen-enhanced localized plasticity—a mechanism for hydrogen-related fracture.* Materials Science and Engineering: A, 1994. **176**(1-2): p. 191-202.
42. Neeraj, T., R. Srinivasan, and J. Li, *Hydrogen embrittlement of ferritic steels: Observations on deformation microstructure, nanoscale dimples and failure by nanovoiding.* Acta Materialia, 2012. **60**(13-14): p. 5160-5171.
43. Nagumo, M. and K. Takai, *The predominant role of strain-induced vacancies in hydrogen embrittlement of steels: Overview.* Acta Materialia, 2019. **165**: p. 722-733.
44. Martin, M., I. Robertson, and P. Sofronis, *Interpreting hydrogen-induced fracture surfaces in terms of deformation processes: A new approach.* Acta Materialia, 2011. **59**(9): p. 3680-3687.
45. Abson, D., *Acicular ferrite and bainite in C–Mn and low-alloy steel arc weld metals.* Science and Technology of Welding and Joining, 2018. **23**(8): p. 635-648.
46. Bhadeshia, H. and L. Svensson, *Modelling the evolution of microstructure in steel weld metal.* Mathematical modelling of weld phenomena, 1993. **1**: p. 109-182.
47. Sharma, S.K. and S. Maheshwari, *A review on welding of high strength oil and gas pipeline steels.* Journal of Natural Gas Science and Engineering, 2017. **38**: p. 203-217.
48. Layus, P., et al., *Study of the sensitivity of high-strength cold-resistant shipbuilding steels to thermal cycle of arc welding.* International journal of mechanical and materials engineering, 2018. **13**(1): p. 1-9.
49. Guillal, A., et al., *Effects of martensite-austenite constituents on mechanical properties of heat affected zone in high strength pipeline steels-review.* Chem Eng Trans, 2018. **70**.
50. Ito, Y. and M. Nakanishi, *Study of the properties of weld metal with submerged arc welding.* The Sumitomo Search, 1976. **15**: p. 42-62.
51. Sabokrouh, M., S. Hashemi, and M. Farahani, *Experimental study of the weld microstructure properties in assembling of natural gas transmission pipelines.* Proceedings of the Institution of Mechanical Engineers, Part B: Journal of Engineering Manufacture, 2017. **231**(6): p. 1039-1047.
52. Zhu, Z., J. Han, and H. Li, *Effect of alloy design on improving toughness for X70 steel during welding.* Materials & Design, 2015. **88**: p. 1326-1333.
53. Sheykh Jaberi, F. and A. Kokabi, *Influence of nickel and manganese on microstructure and mechanical properties of shielded metal arc-welded API-X80 steel.* Journal of materials engineering and performance, 2012. **21**: p. 1447-1454.
54. Frantov, I., et al., *Weldability of niobium-containing high-strength steel for pipelines.* Welding journal, 2014. **93**(1): p. 23-9.
55. Zhang, T., et al., *Effect of microstructure inhomogeneity on hydrogen embrittlement susceptibility of X80 welding HAZ under pressurized gaseous hydrogen.* International Journal of Hydrogen Energy, 2017. **42**(39): p. 25102-25113.
56. Qu, J., et al., *Hydrogen-assisted crack growth in the heat-affected zone of X80 steels during in situ hydrogen charging.* Materials, 2019. **12**(16): p. 2575.
57. Álvarez, G., et al., *Hydrogen embrittlement of structural steels: Effect of the displacement rate on the fracture toughness of high-pressure hydrogen pre-charged samples.* International Journal of Hydrogen Energy, 2019. **44**(29): p. 15634-15643.

58. Drexler, E.S., et al., *Apparatus for accelerating measurements of environmentally assisted fatigue crack growth at low frequency.* Experimental Techniques, 2014.
59. ASME, *Boilder and Pressure Vessel Code*, in *VIII*. 2007, ASME.
60. Nibur, K.A., Somerday, B.P., San Marchi, C., Foulk, J.W., Dadfarnia, M., Sofronis, P., *The relationship between crack-tip strain and subcritical cracking thresholds for steels in high-pressure hydrogen gas.* Metallurgical and Materials Transactions A, 2013. **44**(1): p. 248-269.
61. Stalheim, D., et al. *Optimization of Through Thickness Microstructural Grain Size, Homogeneity and Niobium Metallurgy Performance for Cost Effective Improved API X80 Heavy Gauge Large Diameter Pipe Body and Weld Mechanical Property Stability*. in *International Pipeline Conference*. 2022. American Society of Mechanical Engineers.